Contents

List of Figures

List of Tables

1. Theoretical foundation

This section is inspired from [5]. It briefly treats the main theoretical foundations needed to perform this experiment and to evaluate the collected data.

1.1. Gaussian beams

Gaussian beams are a common model to describe the propagation and properties of laser beams. Perpendicular to the axis of propagation, the beam has a Gaussian profile where as it is Lorentz shaped in the direction of propagation.
In cylindrical coordinates one can use

$$I(r,z) = I_0 \left(\frac{w_0}{w(z)}\right)^2 e^{-2\left(\frac{r}{w(z)}\right)^2} \tag{1.1}$$

where z is the direction of propagation, r the distance from the z-axis, $w(z) = w_0\sqrt{1+\left(\frac{z}{z_R}\right)^2}$ the width of the laser in the plane perpendicular to the propagation. Finally $w_0 = \frac{\lambda f}{\pi w_l}$ is the width of the beam in focus with f the focal length of a lens, w_l the diameter of the laser at the lens and λ the wavelength of the laser, as can be seen in Fig. 1.1. In addition $z_R = \frac{\pi w_0^2}{\lambda}$ is called the Rayleigh length, which is

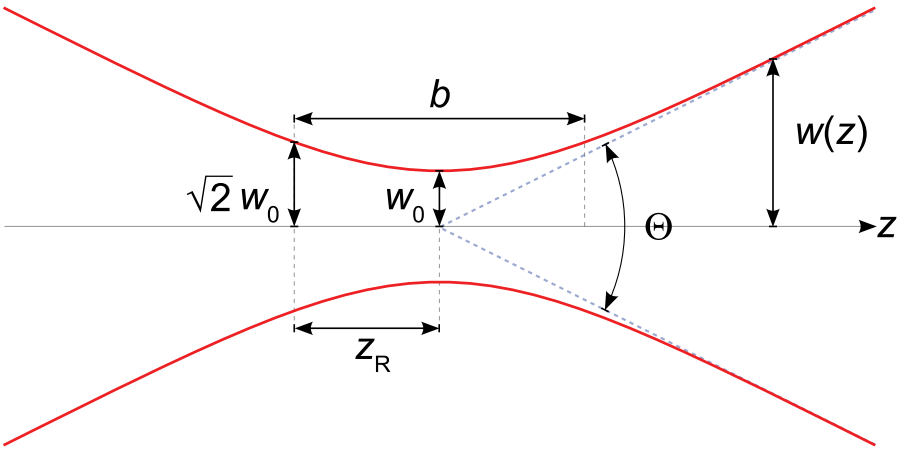

Fig. 1.1.: Focal region of a gaussian laser beam.
source: https://en.wikipedia.org/wiki/Gaussian_beam, accessed: 24.06.2020, 11:28

the distance in z-direction from the focal point (z=0) at which the laser intensity $I(r, \pm z_R) = \frac{1}{2}I_0$ has dropped to half of its maximum $I_0 = I(r = 0, z = 0)$.

1.2. Potassium

In this experiment one observes the electron configuration of potassium. Therefor ^{39}K is used, which is the most abundant natural potassium isotope (93.26%). Since

it is an alkali metal, it is highly reactive. Even contact with air humidity will lead to a dangerous exothermic reaction. Furthermore this contact would lead to the formation of an oxide shell around the elementary substance, thus rendering it unusable for the purpose of this measurement. Therefor the potassium is kept under high vacuum conditions. A level scheme of the transitions of ^{39}K can be found in Fig. 1.2.

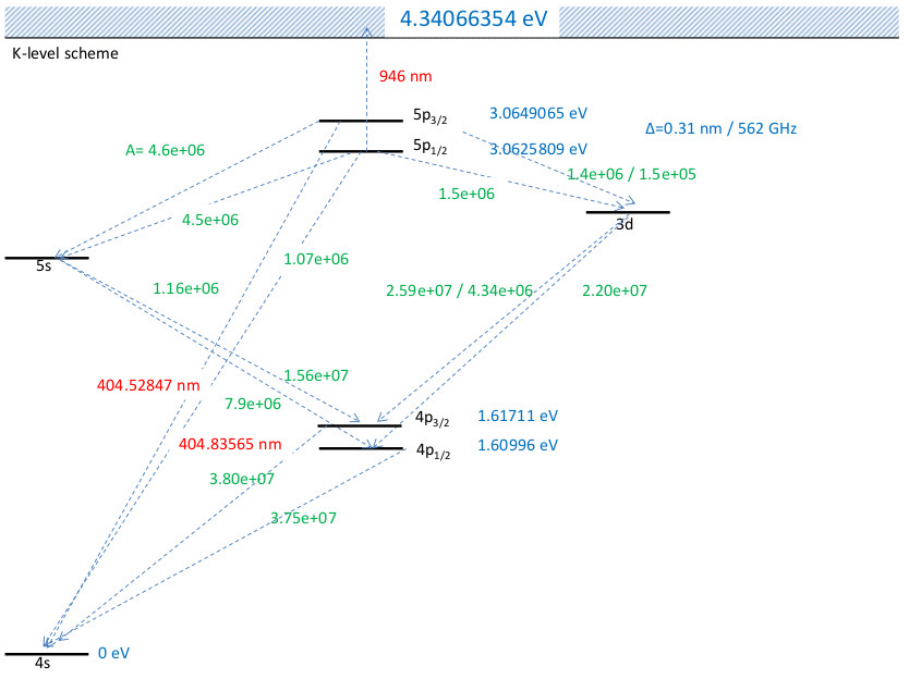

Fig. 1.2.: Level scheme of potassium, taken from [3]

1.3. VMI/SMI spectroscopy

The setup utilized in this study can be operated in two different modes:
The first is the VMI-mode, where the velocity distribution of charged particles in a volume can be observed, independent of the spatial starting configuration of the particles.
The second is the SMI-mode, where the spatial distribution of the charged particles is mapped onto the surface of the spectrometer independent of the velocity distribution.
The spectrometer consists of electrodes after the Eppink-Parker-Design. The repeller is the lowest electrode, followed by the extractor and the ground electrode which both have circular holes in them. The ground electrode ensures a field free drift zone towards the detector surface, while the other two electrodes are used to accelerate the particles. An example of a Eppink-Parker-Design can be found in Fig. 1.3. The different operation modes are achieved by varying the ratio between the repeller and extractor voltages.
The whole experimental setup and its single components will be inspected more thoroughly later in the next chapter.

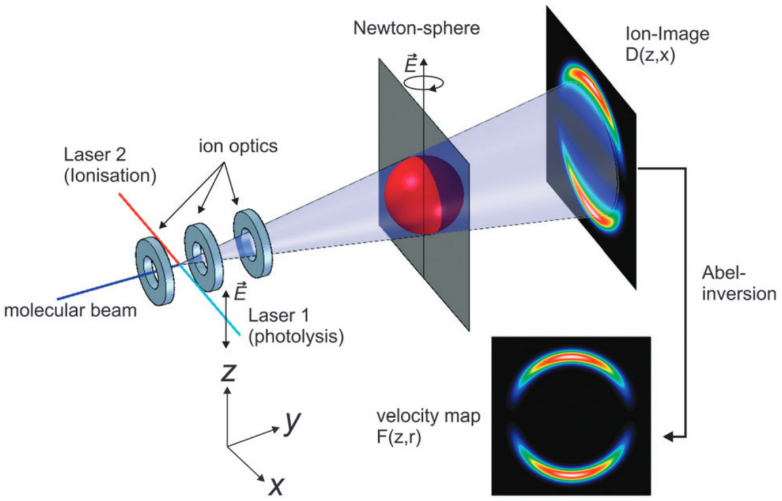

Fig. 1.3.: Schematic setup of an ion imaging experiment, showing the relation of the Newton sphere to the velocity map and the ion image. The axis system used is also indicated. [2]

1.4. Velocity distribution and Abel Inversion

In order to visualize the distributions, the charged particles are accelerated toward a phosphor screen. Consequentially the observed 3D distribution is mapped on a 2D surface. However one can still extract information of the initial 3D configuration out of the mapped image.
For this we first utilize the fact, that a linearly polarized laser marks the photo ionization in one spacial direction. In regards to this axis, the velocity distribution exhibits a cylindrical symmetry. Afterwards one uses calculus as will be shown here after. Looking at the case where the polarization direction is parallel to the detector

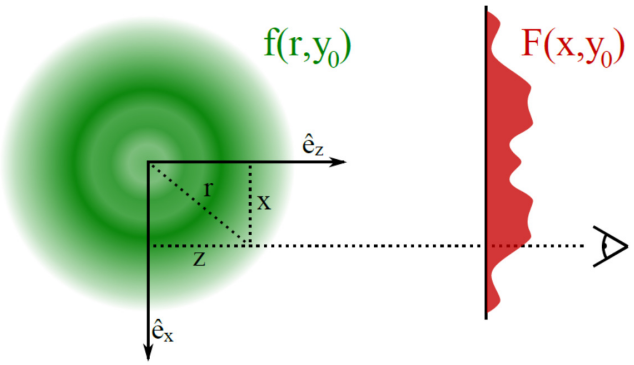

Fig. 1.4.: In this sketch cuts through the distributions $f(r, y)$ and $F(x, y)$ are plotted for fixed $y = y_0$. The observer has a look on the distribution along the z-axis [3]

plane, one obtains a symmetric velocity distribution $f(r, y)$ along the $y-$axis. This then yields a projection $F(x, y)$ on the detector surface. If an infinitely far away observer would now look at the screen along the z-direction, he or she would see

this projection, which is the, along the z-axis, integrated distribution $f(r,z)$:

$$F(x,y) = 2\int_0^\infty f(r,y)\mathrm{d}z \tag{1.2}$$

Knowing that $r^2 = x^2 + y^2$ yields:

$$\mathrm{d}z = \frac{r}{\sqrt{r^2 - x^2}}\mathrm{d}r \tag{1.3}$$

By substitution one arrives at

$$F(x,y) = 2\int_{|x|}^\infty \frac{f(r,y)r}{\sqrt{r^2 - x^2}}\mathrm{d}r \tag{1.4}$$

which is called the Abel-transform. for a visualization of this, see figure 1.4.
Now in this experiment, only $F(x,y)$ can be measured but $f(r,y)$ is the real item of interest. To this end we employ trick, called the Inverse-Abel-transform, which has the form:

$$f(r,y) = -\frac{1}{\pi}\int_{|r|}^\infty \frac{\mathrm{d}F(x,y)}{\mathrm{d}x}\frac{1}{\sqrt{x^2 - r^2}}\mathrm{d}x \tag{1.5}$$

The problem with this formula is, that it assume a continuous distribution, which the measured data will not provide. It will be discrete due to the finite number and size of the pixel in the CCD-camera.
This is where the BASEX-method (**B**asis **S**et **EX**pansion) comes into play, which provides a numerical approach to solve the integral 1.5. The main idea of the approach is the use of so-called basisfunctions $\bar{f}_k$ in the space of distributions f. The projections of these basis functions $\bar{F}_k$ should be well known. They can be chosen arbitrarily but need to fulfill the following three conditions:

- every function should be easily analytically integrable to perform the Abel-transformation
- intensity-distributions obtained by this transformation shall permit imaging of sufficiently small structures
- the projections shall be sufficiently smooth on even smaller distances

The base used in this case is

$$\bar{f}_k = \left(\frac{e}{k^2}\right)^{k^2}\left(\frac{r}{\sigma}\right)^{2k^2}\exp(-\left(\frac{r}{\sigma}\right)^2) \tag{1.6}$$

with σ being the position of the maxima and the spread of the function over r.
The respective Abel-transformations are given by:

$$\bar{F}_k(x) = 2\sigma\bar{f}_k(x)\left[1 + \sum_{l=1}^{k^2}\left[\left(\frac{x}{\sigma}\right)^{-2l}\prod_{m=1}^{l}\left(\frac{(k^2+1-m)(m-0.5)}{m}\right)\right]\right] \tag{1.7}$$

Since the Abel-transformation is a linear transformation, the $\bar{F}_k$ provide a basis in the space of projections and every measured image can be expressed as a linear combination of the $\bar{F}_k$. A visualization of the basis functions and their projections is shown in Fig. 1.5

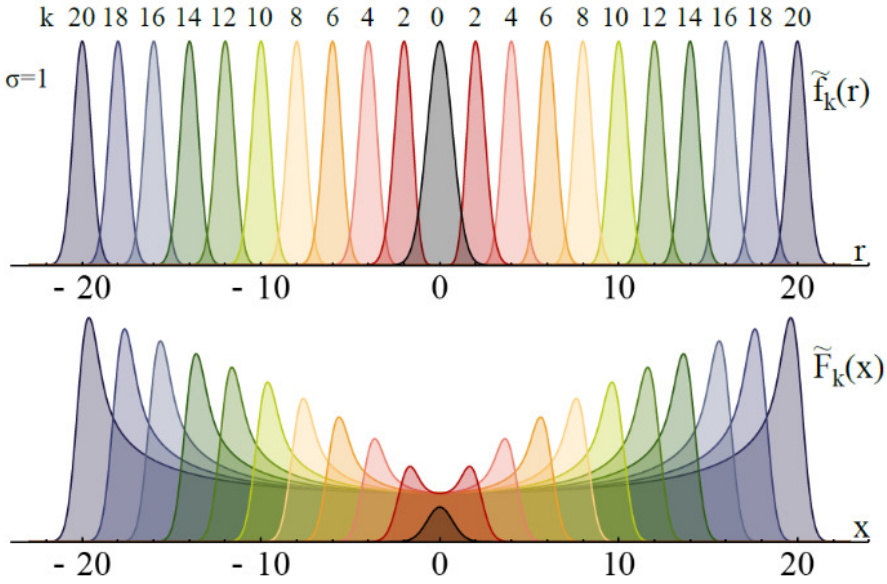

Fig. 1.5.: The basis functions $\bar{f}_k$ (top) used in the BASEX-method, and their projections (bottom). [3]

1.4.1. The Anisotropy-Parameter and REMPI

In an ensemble of atoms, in this case the K-atoms inside the ionization volume, the directions of the orbital angular momenta are oriented arbitrarily. Using a linear polarized laser for ionization, one obtains all possible projections of the orbital angular momenta in the direction of polarization. Hence the measured distribution for the absorption polarized photons $J_{nl}(\theta)$ is the average of all distributions $J_{nlm}(\theta, \phi)$. For one photon one gets:

$$J_{nl}(\theta) = 1 + \beta P_2(\cos(\theta)) \tag{1.8}$$

Here P_2 is the second Legendre polynomial and β is the anisotropy-paramter. They are given by:

$$P_2(x) = 1.5x^2 - 0.5 \quad \text{and} \quad \beta \in [-1, 2] \tag{1.9}$$

Besides ionizing an atom with one photon, also multiple photon ionization is possible. The ground state of ^{39}K being the $4s_{1/2}$ configuration would take multiple photons hitting an atom at the same time to ionize. Luckily, the ground state can be excited with a commercial laser, with wavelength of 404.5 nm, to the $5p_{3/2}$ state from which it can then be ionized by a photon of the same wavelength. This process is called **R**esonant **E**nhanced **M**ulti **P**hoton **I**onization. Even if the electrons excited to the $5p_{3/2}$ state relax into a lower state, they can still be ionized by 404.5 nm wavelength photons with reasonable efficiency. Fig. 1.6 illustrates the various ionization paths with photons of the mentioned wavelength.
This process is much more efficient, than single photon ionization. Since it requires two photons, it also needs a two photon anisotropy-factor which is given by:

$$J_{nl}(\theta) = 1 + \beta_2 P_2(\cos\theta) + \beta_4 P_4(\cos(\theta)) \tag{1.10}$$

where $P_4 = 4.375x^4 - 3.75x^2 + 0.375$ is the fourth Legendre polynomial.

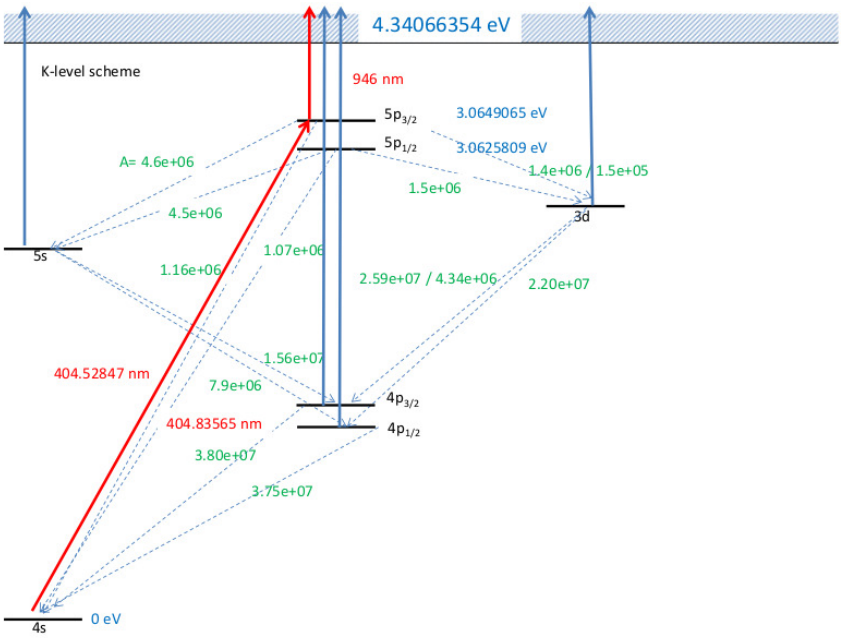

Fig. 1.6.: Level scheme of a REMPI path: $4s_{1/2} \rightarrow 5p_{3/2} \rightarrow K^+$

2. Setup

In this chapter a closer look will be taken at the different components of the experimental Setup, of which a sketch can be seen in Fig. 2.1.

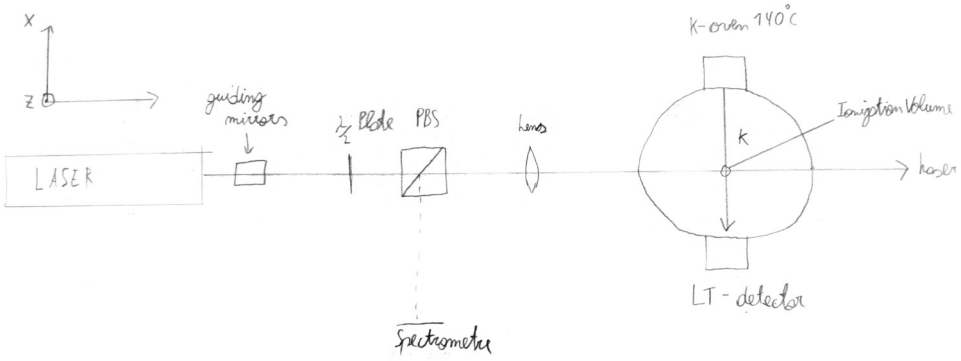

Fig. 2.1.: Sketch of the beam path of the VMI experiment

2.1. Laser system

The laser utilized in this setup is a "Topica DL pro" single mode tunable diode laser. It is tunable by three different mechanisms namely:

- One can tune the frequency of the laser diode by changing the current that feeds the diode
- Behind the laser diode, a grit is mounted in the Littrow configuration onto the beam in a way, that the first order reflection of the grid is reflected back into the diode. Since a laser diode is very sensitive to light falling onto it, variation

of the angle of the grid, one can vary the frequency which is reflected back into the diode. The frequency of reflected light from a grid is dependent on the incoming angle of the light.

- The laser can also be tuned by changing the temperature of the diode which influences the band gap of the semiconductor material and therefore changes the frequency of the emitted light.

2.2. Optical elements

In the following the optical elements installed in the beam path will be explained.

Guiding mirrors Mirrors used to guide the laser beam through the other optical elements and into the cavity in a way that the beam is parallel to the cavity.

$\frac{\lambda}{2}$-plate This plate consists of an anisotropic optical material. It has different refractive indices for the ordinary and the extraordinary beam. Both undergo a phase shift while traveling through the plate. One now can chose the length of the material in a way that the relative shift between the two parts of the beam is $\frac{\lambda}{2}$. This equals a phase shift of π.

Partial beam splitter (PBS) The PBS splits the laser beam in two perpendicularly split beams. The perpendicular part of the beam is reflected perpendicularly to the beam direction, while the parallel polarized part can pass through. It used to check the polarization behind the $\frac{\lambda}{2}$-plate.

Lens Used to focus the laser beam into the K-atom beam.

2.3. Spectrometer

In the instruction, the use of a K-cell is proposed in order to determine that the laser is tuned to the correct frequency. However the camera observing the K-cell broke, so a spectrometer was installed perpendicular to the PBS, to observe the laser frequency.

2.4. LT-detector

The Langmuir-Taylor-detector is a simple detector for alkali-atoms like potassium. It consists of a glowing rhenium filament and a Faraday-cup. The filament is heated via a current. Its purpose is to measure the amount of K-atoms that are vaporized in the K-oven. The atoms are accelerated towards the LT-detector by two electrodes of which one has a hole. The atoms are ionized by the glowing rhenium via surface ionization. These ions are then accelerated toward the Faraday-cup. The resulting current is measured using a femtoamperemeter from which the flux can be calculated since one knows the area of the filament, which is 6 mm^2.

2.5. K-oven

The thermal K-atoms are provided by solid potassium which is heated in the K-oven. It consist of two resitive heaters inside a copper clamp which is in turn wrapped around the steel container containing the potassium. Since one wants a well collimated beam the oven has a hole of only 2 mm in direction of the interaction region with the laser. The potassium beam has a diameter of approx. 3.5 mm in the ionization volume. The temperature of the oven can be controlled via the applied current and should never exceed 160 °C.

2.6. 2D detector

The 2D detector for the VMI/SMI spectroscopy consists of three components which are showcased in this section. A photo of the detector can be seen in Fig. 2.2

Fig. 2.2.: Picture of the 2D detector on top of the setup [5]

2.6.1. MCP

Two mirco channel plates (MCP) are the top part of the detector. They are made of a highly resistive material and contain small channels which are spaced by 10 µm, have a diameter of 8 µm and are tilted with respect to the MCP's surface. When they are hit by charged particles, electrons are generated. By applying a high voltage (1.7 kV) these electrons are then accelerated toward the back of the MCP where they generate additional electrons. Due to this avalanche effect, an amplification of

around a factor 1000 is achieved by each MCP. A schematic of the component can be seen in Fig. 2.3

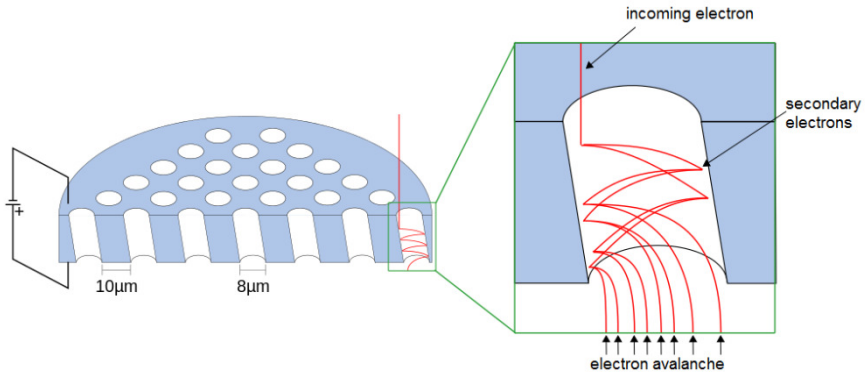

Fig. 2.3.: Schematic of an MCP [3]

2.6.2. Phosphor screen

Behind the MCPs a phosphor screen is installed. The generated electrons are accelerated toward the screen by a voltage of 3.5 kV and cause a flash of light with a wavelength determined by the used screen. The flash decay time for the screen used in this setup is around 4 ms.

2.6.3. CCD Camera

The flashes of light produced by the phosphor screen are then recorded by a CCD camera, which transmits the recorded images to the PC. The exposure and gain of the camera can be controlled with the program “FlyCapture2“.

2.7. Vacuum system

The whole cavity is kept in a continuous vacuum of at least $5 \cdot 10^{-10}$ bar. This is achieved by combining a membrane pump with a turbo-molecular pump. The pressure is monitored by a control unit and displayed on a screen next to the pump system.

3. Procedure

In this section the experimental procedure is described.
The first part in this experiment was to get familiar with VMI and SMI spectroscopy using a simulation program. Using this program, the simulations shown in chapter 4 were generated and analyzed.
Before performing any measurement, the optical alignment of the setup was tested. Therefor the beam size and shape was checked using a piece of paper, at the exit of the laser, after the guiding mirrors, before the vacuum chamber and behind the vacuum chamber. It had the same brightness and diameter at all points and entered the chamber at the same height as it exited it, meaning that the optical alignment was already very satisfactory and any changes would have probably led to a worsening of the beam path qualities.
As a first measurement, the laser was guided inside the K-cell, which is a glass tube equipped with a heating system and potassium inside. The goal was to tune the laser to the right wavelength using the laser controls explained in section 2.1. The right wavelength being the wavelength of the K $5p_{3/2}$ state namely 404.52847 nm. If the correct wavelength of the laser is obtained, a faint line of fluorescent light is to be observed using a camera mounted to observe the tube. Unfortunately the camera broke before the fluorescent light was seen. Therefor this part of the experiment was impossible to execute and the wavelength of the laser was controlled by a spectrometer which was installed instead of the K-cell. The controls of the laser were not tuning the wavelength sufficiently, so the tutor had to manually adjust the grid of the laser with an hexagon screwdriver to get as close to the desired wavelength as possible. The achieved wavelength was at 404.4 nm with a FWHM of 1 nm which was good enough for our purposes.
Next the image ratio of the setup was to be determined. Therefor the voltages of the MCP's and the phosphor screen were set to 1.7 kV and 3.5 kV respectively, where first the MCP's and then the phosphor screen were ramped up, in order to guarantee that the difference in tension between the two components never exceeded 3 kV. Then the repeller voltage was set to 5 kV and the ratio of repeller to extractor voltage was set to the simulated optimal for SMI mode, 89.6%. The position of the lens in front of the chamber was varied, and the resulting SMI pictures were recorded.
Second the optimal ratio for SMI mode was determined by varying the ratio of U_R/U_E and taking 100 pictures for every value of the ratio that was analyzed. Therefor the shutter time of the camera was maximized, leading to minimal exposure time, to avoid saturation of the images and damage to the camera.
Next the atomic flux coming from the K-oven was measured by employing the LT-detector introduced in section 2.4. First the oven was heated to 159.2°C and the voltages on the electrodes of the LT-detector were adjusted to yield maximal current. We got an extractor voltage of 7.9 V and a repeller voltage of 14.9 V. Then the heater of the K-oven was shut down, and the current was written down as a function of the

decreasing temperature.
After this measurement, the same measurement as was done for the SMI optimal ratio was now repeated for the VMI mode, only the polarity of the electrodes was switched at 0 V.
Last a background image was recorded, where only laser, MCP and phosphor screen were turned on, but the reppeler and extractor electrodes stayed switched off.

4. Simulations

Before the experiment itself is performed, some simulations are done. For this the software *Simion 8.0* [1] is used and the geometry of the spectrometer is implemented.

4.1. Simulation for the VMI-mode

To perform velocity map imaging it is necessary that two electrons with the same velocity vector during ionization are found at the same spot on the detector. This is highly dependent on the voltage ratio between the repeller and the extractor electrode. Thus, before doing the actual experiment, some simulations with two electrons with initial distance $d = 1\,\text{mm}$, initial velocity vector $\boldsymbol{v} = (1, 0, 0)$ and kinetic energy of $0.1\,\text{eV}$ are performed. In order to find the optimal ratio more easily, they are set at the initial points $\boldsymbol{x}_1^{\text{ini}} = (0, -0.5, 0)$ and $\boldsymbol{x}_2^{\text{ini}} = (0, 0.5, 0)$. The advantage of this start configuration is that the points in which the electrons hit the detector are symmetric, thus the distance Δd on the detector is given by $\Delta d = \left|2y_1^{\text{det}}\right|$ as there is no acceleration in the z-direction. The superscript "det" indicates the position on the detector.
In all simulations the voltage of the repeller electrode is held constant at $-3\,\text{kV}$ while the voltage of the extractor electrode is changing. The different voltages and their resulting y^{det} values can be found in Tab. 1 in Appendix A and are plotted in Fig. 4.1.
In the area of the minimal distance between the electrons on the detector one can expect the dependence on the voltage ratio to be linear. Thus a linear fit is applied between $70\% \leq U_E/U_R \leq 78\%$ which can be seen in Fig. 4.2. The resulting optimal ratio is

$$\frac{U_E}{U_R} = 72.688(5)\,\%$$

As the measurements were only simulations the error of this quantity should not be regarded.
It should be noted that the distance at this voltage ratio should not be 0 as the electrons will repel each other for extremely small distances, but this effect is negligible.
Next the dependence on the repeller voltage is checked. Therefor the same simulation with six different U_R but at optimal voltage ratio are done. The results which can be seen in Appendix A Tab. 2 show no dependence. Hence one only needs to look at the voltage ratio but U_R can be chosen freely.

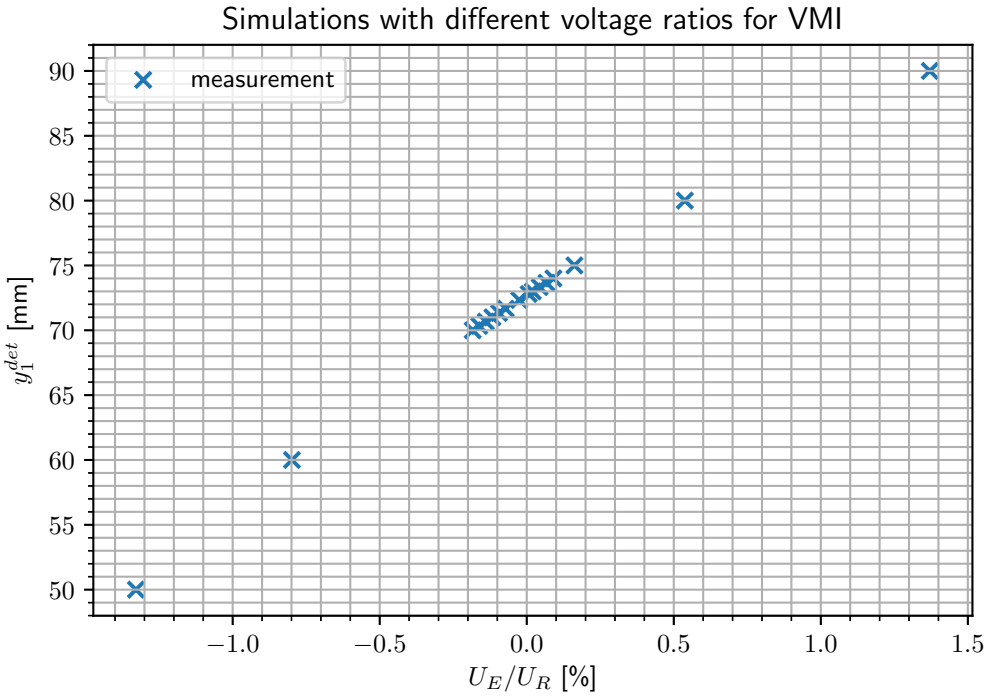

Fig. 4.1.: The voltage ratios U_E/U_R are plotted over y_1^{det} to find the ratio that minimizes the difference between the electrons on the detector.

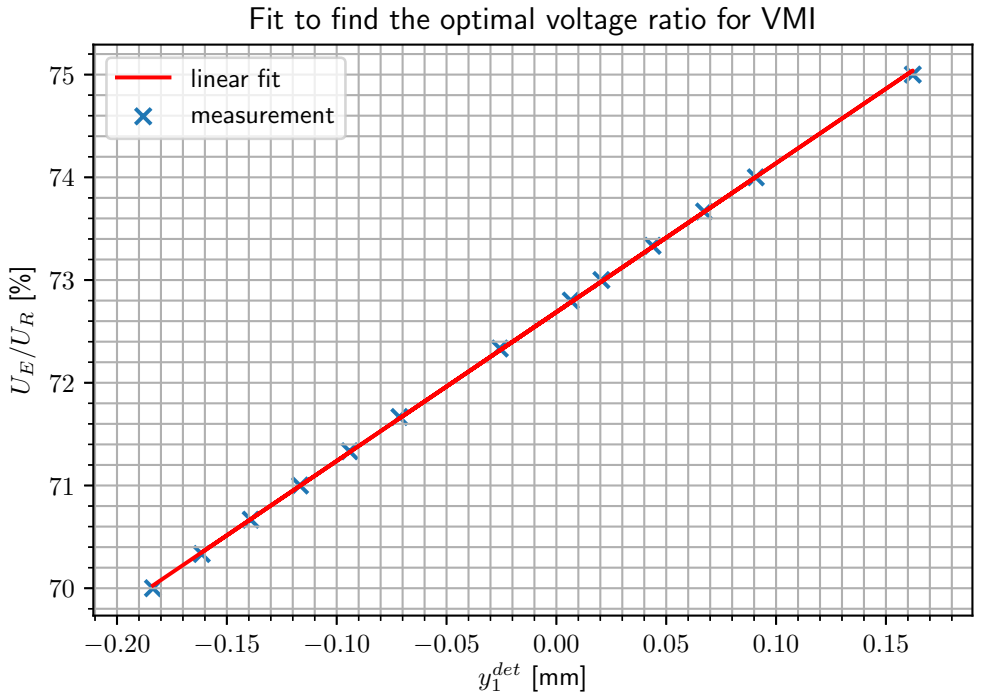

Fig. 4.2.: Around the expected minimum a line is fitted to receive the optimal voltage ratio.

4.2. Simulation for the SMI-mode

For spatial map imaging it is necessary that two K-ions with the same initial position are mapped at the same spot on the detector. This also depends on the voltage ratio between the repeller and the extractor electrode. Thus some simulations with two K-ions with initial position $\boldsymbol{x}^{\text{ini}} = (0, 0, 0)$ and kinetic energy of 0.1 eV are performed. The initial velocity vectors are $\boldsymbol{v}_1^{\text{ini}} = (0, 1, 0)$ and $\boldsymbol{v}_2^{\text{ini}} = (0, -1, 0)$. Again the points in which the ions hit the detector are symmetric, thus the distance Δd on the detector is given by $\Delta d = \left|2y_1^{det}\right|$.
In all simulations the voltage of the repeller electrode is held constant at 3 kV while the voltage of the extractor electrode is changed. The different voltages and their resulting y^{det} values can be found in Tab. 3 in Appendix A and are plotted in Fig. 4.3.
Analogously to 4.1 a linear fit between $91\% \leq U_E/U_R \leq 92\%$ is applied which can be seen in Fig. 4.4. The resulting optimal ratio is

$$\frac{U_E}{U_R} = 91.6030(14)\,\%$$

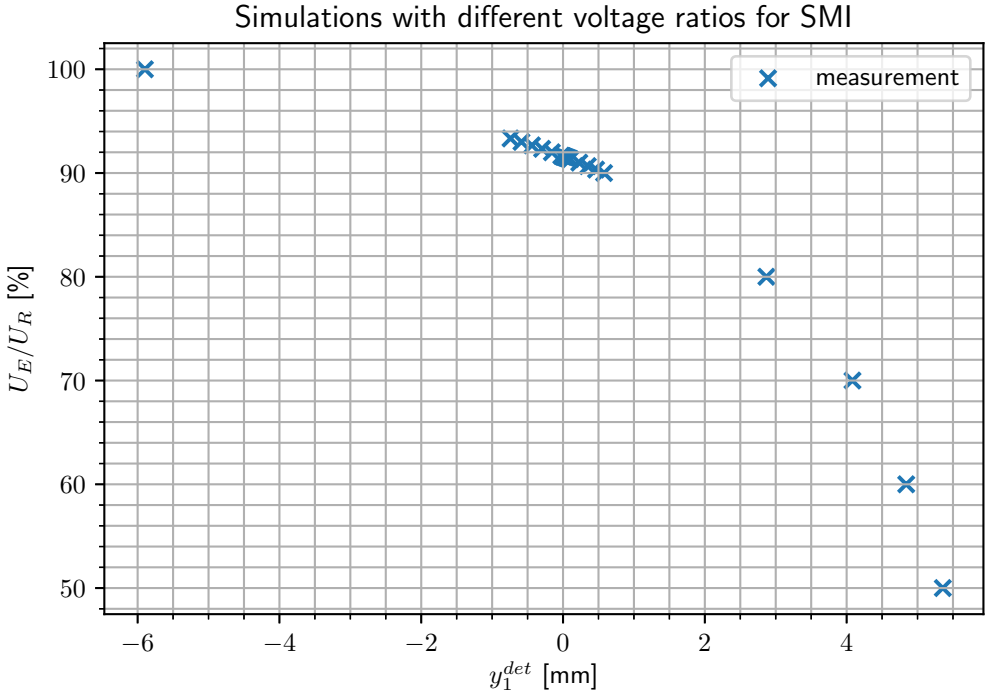

Fig. 4.3.: The voltage ratios U_E/U_R are plotted over y_1^{det} to find the ratio that minimizes the difference between the ion on the detector.

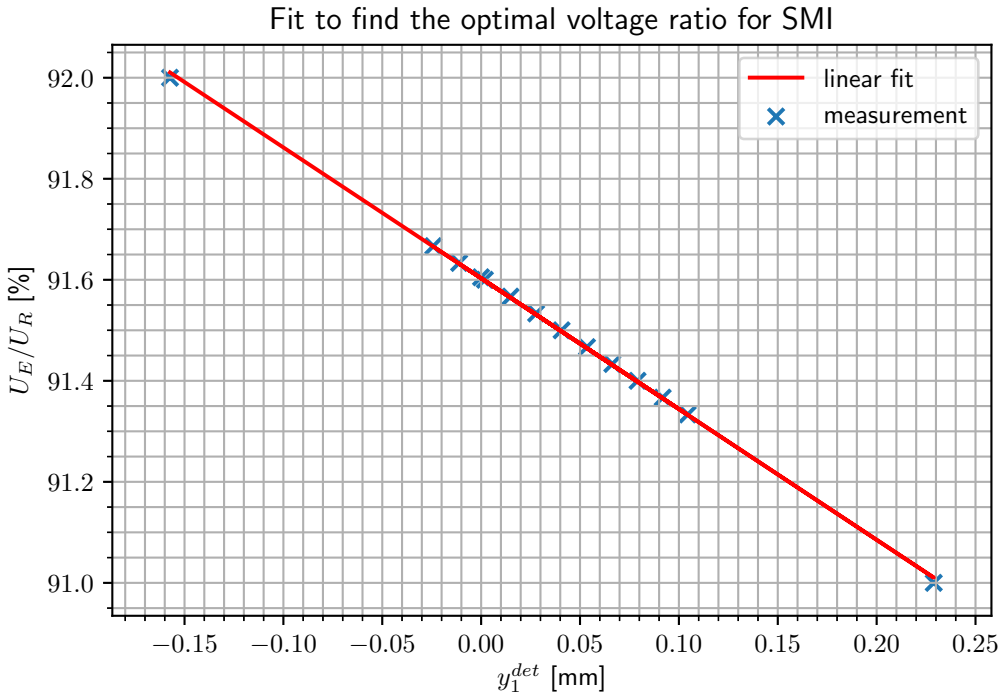

Fig. 4.4.: Around the expected minimum a line is fitted to receive the optimal voltage ratio.

4.3. Simulation for different initial velocities

It is interesting how electrons with different velocity vectors are presented on the detector. Thus for each of the three different kinetic energies $E = 4, 2, 1$ eV 500 electrons with spherical distributed initial velocity vectors and same initial position vector $\boldsymbol{x}^{\text{ini}} = (0, 0, 0)$ are simulated. The resulting picture on the detector can be seen in Fig. 4.5. Each bunch of electrons forms their own circle. The higher the initial kinetic energy the bigger the radius of the circle.

4.4. Simulation of a particle cloud that represents the ionization volume

Finally a particle cloud that represents the ionization volume is simulated with the SMI settings. For that the beam parameters are computed according to the formulae in section 1.1

$$w_0 = \frac{\lambda \cdot f}{\pi \cdot w_l} = 19.35\,\mu\text{m}$$
$$z_R = \frac{\pi w_0^2}{\lambda} = 2.901\,\text{mm}$$

with $\lambda_{\text{laser}} = 405\,\text{nm}$, $f = 150\,\text{mm}$ and $w_l = 1\,\text{mm}$. The resulting image on the detector can be seen in Fig. 4.6. However, in the experiment the laser was tuned to $\lambda_{\text{laser}} = 404.4(4)\,\text{nm}$. This means that the expected beam waist and Rayleigh length

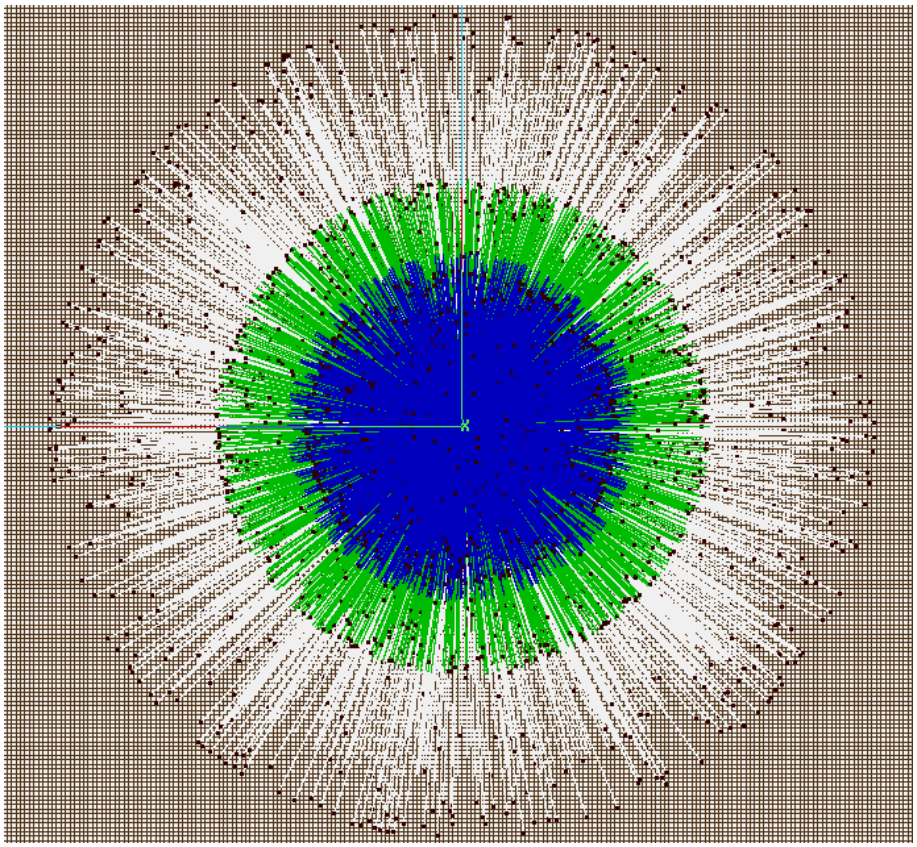

Fig. 4.5.: Simualtion of three bunches of electrons with different kinetic energies. White: 4 eV, green: 2 eV, blue: 1 eV. Shown is the picture from the detector.

under the above assumption are:

$$w_0 = 19.31(2)\,\mu\text{m}, \qquad z_R = \frac{\lambda_{\text{laser}} \cdot f^2}{\pi \cdot w_l^2} = 2.896(3)\,\text{mm}$$

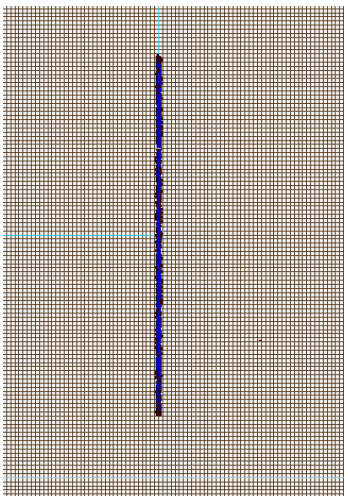

Fig. 4.6.: Resulting image on the detector when a particle cloud that represents the ionization volume is simulated using the SMI settings.

5. Analysis and discussion

5.1. Atom beam detector

In this experiment it is not necessary to know exactly how many K-atoms are coming out of the oven as long as it does not vary too much. Thus the atomic flux is measured over a temperature span of $115\,°\mathrm{C} \leq T \leq 159\,°\mathrm{C}$. The intensity is calculated via

$$J = \frac{I}{e \cdot A_{\mathrm{Re}}}$$

with e the electric charge, I the measured current and $A_{\mathrm{Re}} = 6\,\mathrm{mm}^2$ the area of the rhenium filament. In Fig. 5.1 one can this graphical. The uncertainties are $s_T = 0.2\,\mathrm{K}$ and $s_J = 1 \cdot 10^8\,\mathrm{atoms/smm}^2$. The shape is quite exponential and explodes for temperature that are close to 160 °C. It is reasonable to perform experiments around 140 °C as the flux is sufficiently strong with an intensity of $J \approx 5.5 \cdot 10^8\,\mathrm{atoms/mm}^2\mathrm{s}$ and the slope is not too steep.

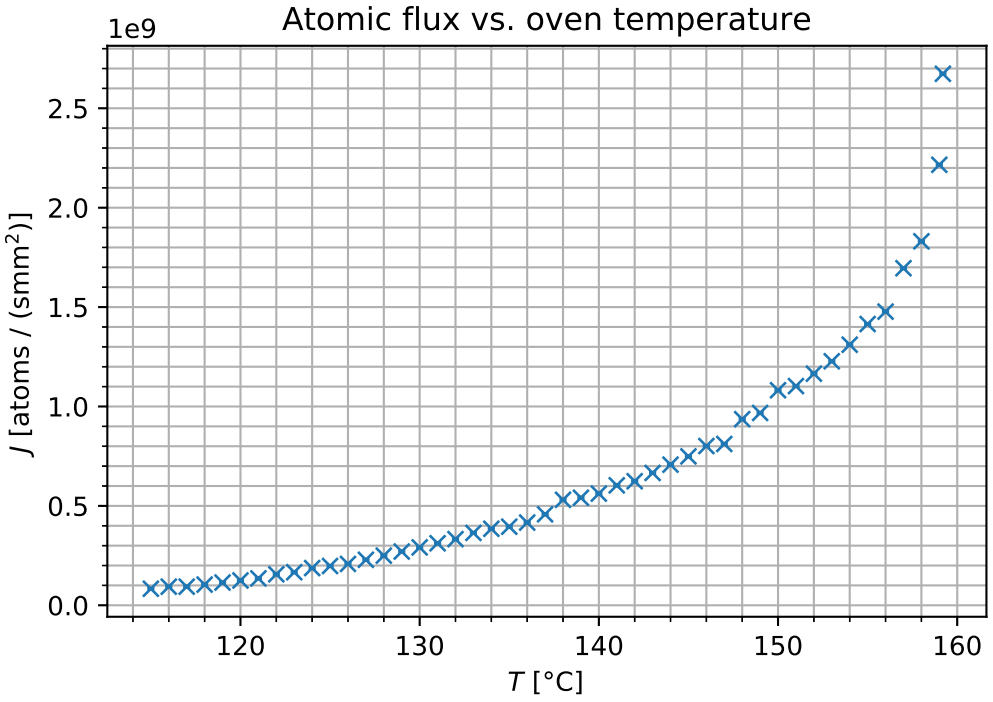

Fig. 5.1.: The atomic flux over the K-oven temperature. It can be seen that the flux has an exponential form.

Due to the visible trend it seems likely that the uncertainties were estimated too low. Especially between $138\,°\mathrm{C} \leq T \leq 159\,°\mathrm{C}$ there seems to be a deviation from

the highly suspected exponential trend of the curve. Thus it might have been more reasonable to estimate relative uncertainties.
For the temperature one has to keep in mind that it is possible that there is a delay on the display. Also, it could be that the LT-detector is not adjusted perfectly. These are systematic uncertainties which cannot be estimated properly.

5.2. Spatial Map Imaging with ions

For the SMI setting one can determine the image ratio of the setup, the optimal ratio U_E/U_R and the dimension of the focal area.

5.2.1. Image ratio of the setup

By varying the position of the lens in the setup one gets different lines on the detector. As the only interesting parts displayed on the detector are the lines, the images, where the background is subtracted, are cropped, added together and can be seen in Fig. 5.2. It should be noted that one measured line is left out, namely the one with the lens position $x = 5.14\,\text{mm}$. This is done because later only the differences between the lens positions are relevant and this position artificially increases the uncertainty on the image ratio since all other positions are in distances of 0.5 mm to each other and a smaller distance would lead to a bigger relative uncertainty which would then be propagated.

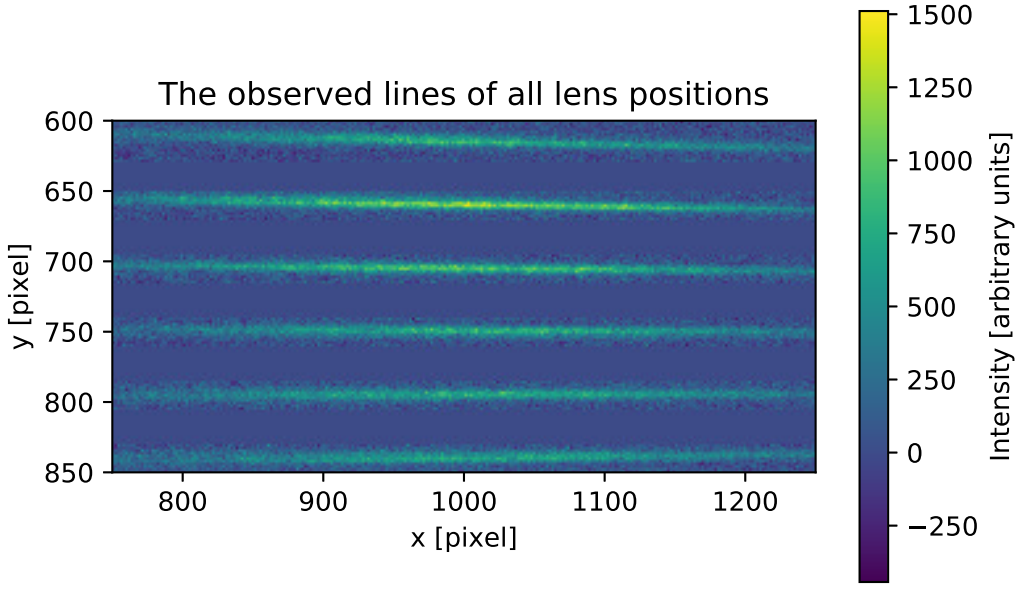

Fig. 5.2.: Image section of the cropped and added pictures at all lens positions. The whole picture has a size of 1200 x 1920 pixels. The lines correspond to lens positions of (top to bottom): 4.5 mm, 5 mm, 5.5 mm, 6 mm, 6.5 mm, 7 mm

For each line the brightest point is selected. Next, vertical cuts are applied to the lines. As the lines are not perfectly horizontal, the slope of the line is estimated and with the gained slope and the known brightest point the vertical cut can be performed. This can be seen in appendix C.2. Afterwards a Gaussian is applied to get the y positions of the peaks. In Fig. 5.3 the fits and their horizontal positions can be seen. The resulting means and their standard deviations can be found in Tab. B.1. With the known differences between the lens positions Δx and the resulting differences on the detector Δd, the image ratio and its error can be computed via

$$B = \frac{\Delta d}{\Delta x}, \qquad \frac{s_B}{B} = \sqrt{\left(\frac{s_{\Delta x}}{\Delta x}\right)^2 + \left(\frac{s_{\Delta d}}{\Delta d}\right)^2}.$$

The image ratios can be found in B.2 and averaging over them yields

$$\bar{B} = 89.8(7)\,\mathrm{px/mm}.$$

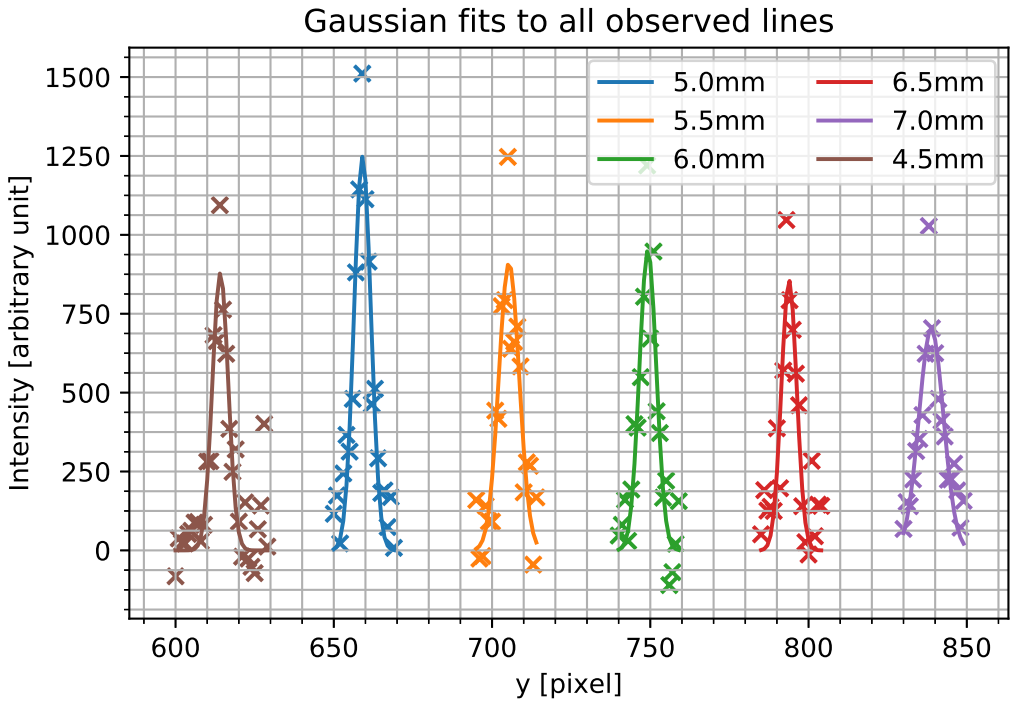

Fig. 5.3.: Gaussian fits to determine the position of the peaks. The x values in the legend indicate the horizontal positions of the vertical cuts.

5.2.2. Optimal ratio for SMI setting

To obtain the optimal ratio for SMI setting, pictures for eight different ratios U_E/U_R have been recorded. The procedure is done analogously to section 5.2.1. To the vertical cuts Gaussians are applied. One example can be seen in Fig. 5.4 for the ratio $U_E/U_R = 89.6\,\%$. The chosen pixels and the fits can be seen in appendix C.3 and the results can be seen in Tab. B.3.

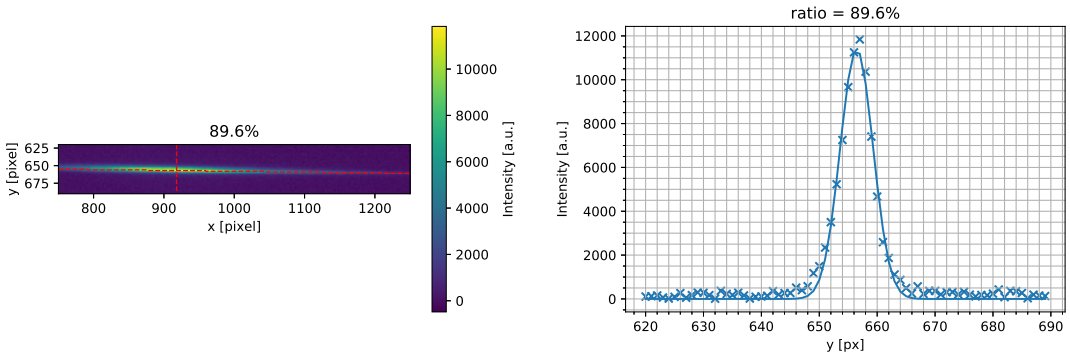

Fig. 5.4.: Method to find the optimal voltage ratio for SMI. In the left picture one can see the pixels chosen for the vertical cut (the pixels along the red vertical line). In the right picture the intensities are plotted over these pixels and a Gaussian is applied.

The standard deviations of the fits are plotted over the ratios in Fig. 5.5. It can be seen that the distribution is already heavily asymmetric thus a quadratic fit does not make any sense. In the region $89\% \leq U_E/U_R \leq 90.5\%$ where it might be justified there are not enough measurements so that the fit would yield useful results and errors. Thus the minimum is simply estimated to be at the ratio which yielded the lowest width:

$$\left(\frac{U_E}{U_R}\right)_{\text{optimal}} = 89.6(4)\,\%$$
$$\sigma_{\text{optimal}} = 2.84(5)\,\text{px}$$

This result has the same magnitude as the simulated optimal ratio $(U_E/U_R)_{\text{simulation}} = 91.6030(14)\,\%$. The difference can be explained by considering, that neither the electrodes nor the voltage suppliers are exactly the same as those implemented in the simulations, thus there could be some systematical error. On the other hand there could be additional statistical errors on the optimal ratio as it is only estimated by eye.

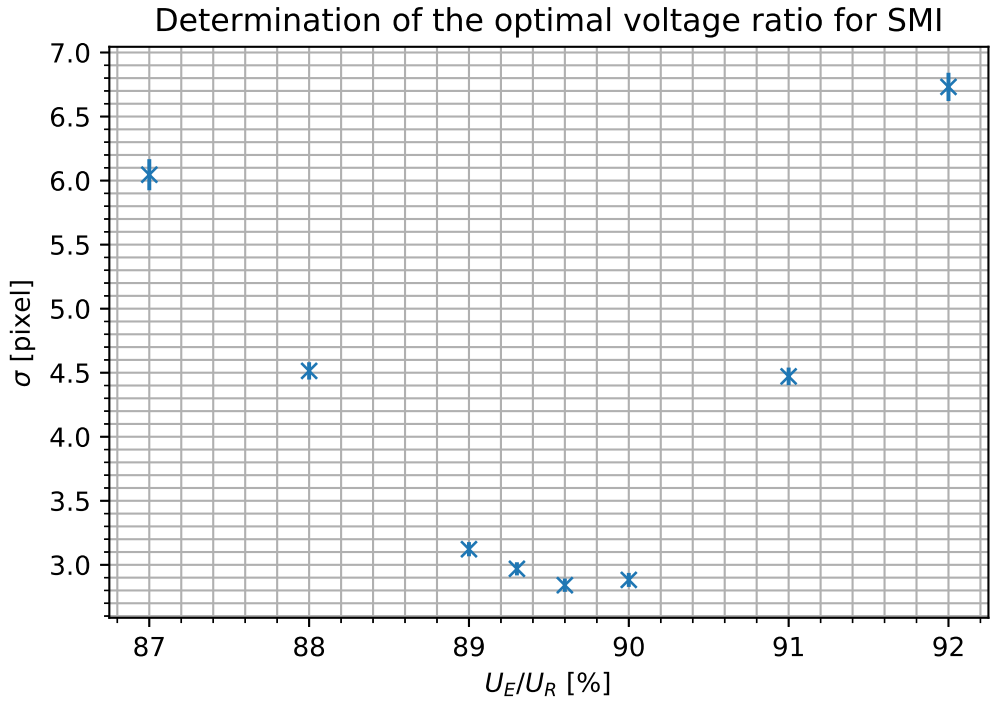

Fig. 5.5.: The standard deviations of the gaussians are plotted over the voltagehas the same magnitude ratios. It can be seen that the total distribution is already asymmetric. Thus a quadratic fit is not justified and in the area where it would be there are not enough points to yield useful results.

5.2.3. Dimensions of the laser focal area

The beam waist and the Rayleigh length are computed via

$$w_0 = \frac{2\sigma_{\text{optimal}}}{\bar{B}} = 63.3(13)\,\mu\text{m}$$
$$z_\text{R} = \frac{\pi w_0^2}{\lambda_\text{laser}} = 31.1(12)\,\text{mm}$$
$$w_l = \frac{\lambda_\text{laser} f}{\pi w_0} = 0.305(6)\,\text{mm}$$

with $\lambda_\text{laser} = 404.4(4)\,\text{nm}$.
A different approach is also tested. Therefor a horizontal cut is applied at the optimal ratio. However, the line on the detector is not completely horizontal thus the cut goes through a line which can be seen in Fig. 5.6. The intensities along this line should follow the distribution

$$I(r=0,z) = I_0 \left(\frac{w_0}{w(z)}\right)^2 = \frac{I_0}{1+\left(\frac{z-z_0}{z_R}\right)^2}$$

which results from (1.1) with $r = 0$. z_0 is the position of the maximum. This function applied to the chosen intensities can be seen in Fig. 5.6 and yield a Rayleigh length

and beam waist of

$$z_R = 1.201(13)\,\text{mm}$$
$$w_0 = 12.43(7)\,\mu\text{m}$$
$$w_l = 1.553(9)\,\text{mm}$$

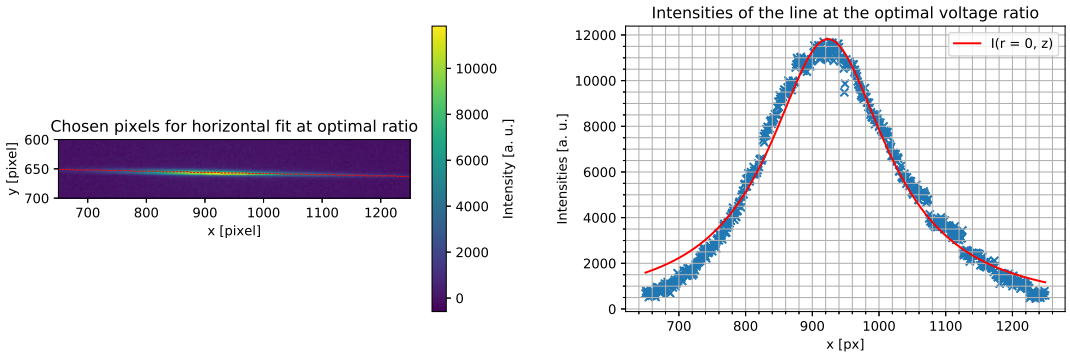

Fig. 5.6.: Method to directly determine the Rayleigh length. In the left picture the intensities in the area $750\,\text{px} \leq x \leq 1250\,\text{px}$, $600\,\text{px} \leq y \leq 700\,\text{px}$ can be seen. The dashed red line indicates the chosen pixels to perform the horizontal fit. In the right picture the horizontal fit at the optimal voltage ratio is plotted.

The different achieved values, which can be seen in Tab. 5.1, are discussed next. None of the values are in agreement with each other. It is remarkable that the magnitude of the parameters from the horizontal fit differs from the vertical fit but has the same magnitude as the calculation. It seems that the vertical fit is not a good choice to measure the beam waist as the laser diameter in front of the lens would only be around a third of a millimeter which does not seem plausible especially if one compares it to the 3x1 mm beam characteristics specified by the manufacturer [1]. On the other hand a diameter of around 1.5 mm seems more reasonable. However, both methods should in general yield the same result if the detector is set to the optimal SMI setting. An idea why the results of these two methods differ so violently from each other could be that since the line on the detector is very narrow it is very sensitive to scattering of photons and Ions around the pixels. Since 100 summed up pictures were used, even very slight vertical translations of the recorded line could have a large impact on the width leading to a larger beam waist. This would of course be negligible in the horizontal fits, which also explains why this method yields results in the expected order of magnitude.

[1] https://www.toptica.com/products/tunable-diode-lasers/ecdl-dfb-lasers/dl-pro/?gclid=CjwKCAjwmrn5BRB2EiwAZgL9otlx-QSEfWboqQc4parq1Wz5Abr-1BoGj2mxCdGzEpuO7SwQxhA6fRoCLhYQAvD_BwE, accessed August 8 2020

Tab. 5.1.: Comparison between the calculated dimensions of the laser focal area and the measured.

	Calculation	Vertical fit	Horizontal fit
w_0 [µm]	19.31(2)	63.3(13)	12.43(7)
z_R [mm]	2.896(3)	31.1(12)	1.201(13)
w_l [mm]	1	0.305(6)	1.553(9)

5.3. Velocity Map Imaging with electrons

For the VMI mode one needs to find the optimal voltage ratio U_E/U_R. At this ratio one can calibrate the photoelectron spectrum, determine the measured transitions and estimate the resolution of the spectrum. Finally the anisotropy parameters are determined.

5.3.1. Optimal ratio for the VMI setting

First the optimal ratio has to be determined. The measured pictures are some sum of the functions with form of the lower half of Fig. 1.5 which can be seen in appendix C.1. Here, instead of finding the FWHM of the measured pictures, the FWHM of the Abel inverted photoelectron spectra are examined. One example can be seen in Fig. 5.7 for the voltage ratio $U_E/U_R = 71.75\,\%$. The other fits can be seen in appendix C.4. The FWHM of all ratios are plotted over the ratios in Fig. 5.8. Again there is no easy pattern recognizable, thus the minimum is only estimated to be at:

$$\left(\frac{U_E}{U_R}\right)_{\text{optimal, VMI}} = 71.8(4)\,\%$$

This result has the same magnitude as the simulated optimal ratio $(U_E/U_R)_{\text{simulation}} = 72.688(5)\,\%$. On one hand the same systematical and statistical error sources as for the SMI optimal ratio hold, namely that neither the electrodes nor the voltage suppliers are exactly the same as those implemented in the simulations and that the optimal ratio is only estimated by eye. On the other hand the inverted pictures are used and their generation is highly dependent on the circular area selected for inversion. This area needs to contain all of the data and needs to be at the center of the circular image. Since the center is only estimated by eye this imposes an additional statistical error source. Furthermore the inversion program assumes the recorded data to have a perfectly circular distribution. This is however not the case as can be seen in Fig. 5.9. The circle is slightly squashed in the y direction which is an additional source for uncertainties.

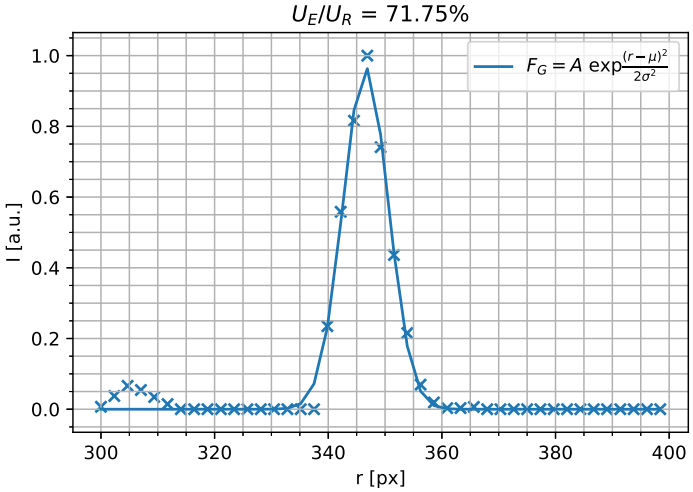

Fig. 5.7.: Method to determine the optimal voltage ratio for VMI. In this picture the PES between $300\,\text{px} \leq r \leq 400\,\text{px}$ can be seen as well as the Gaussian fit that is applied to it. This picture is used as the optimal ratio.

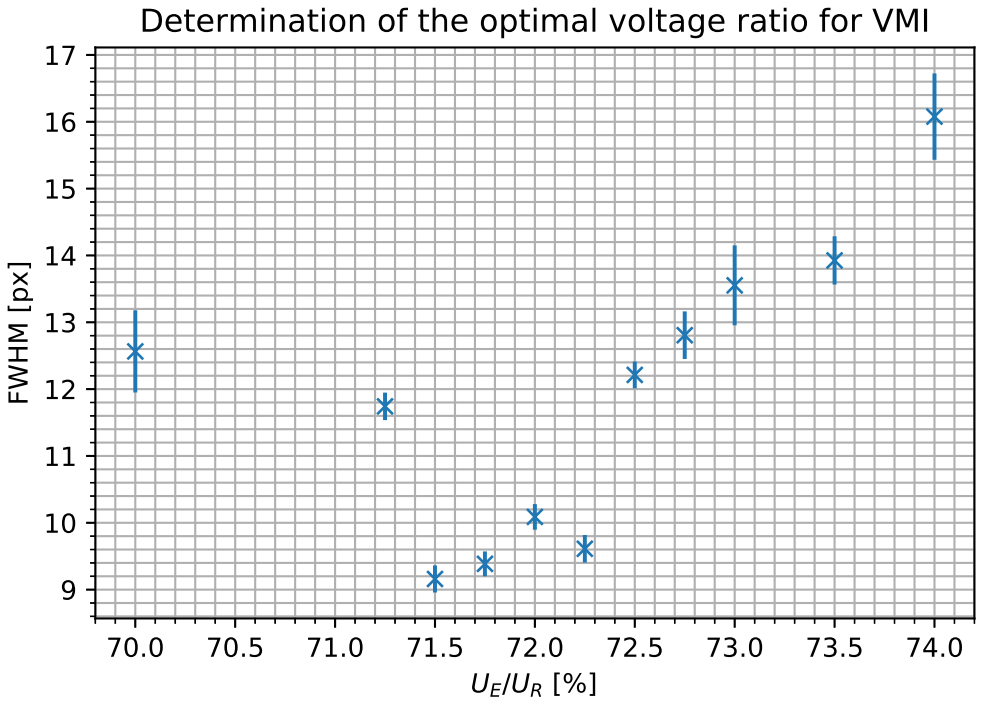

Fig. 5.8.: FWHM of all voltage ratios at the VMI setting. There is no easy pattern recognizable, thus the minimum is only estimated.

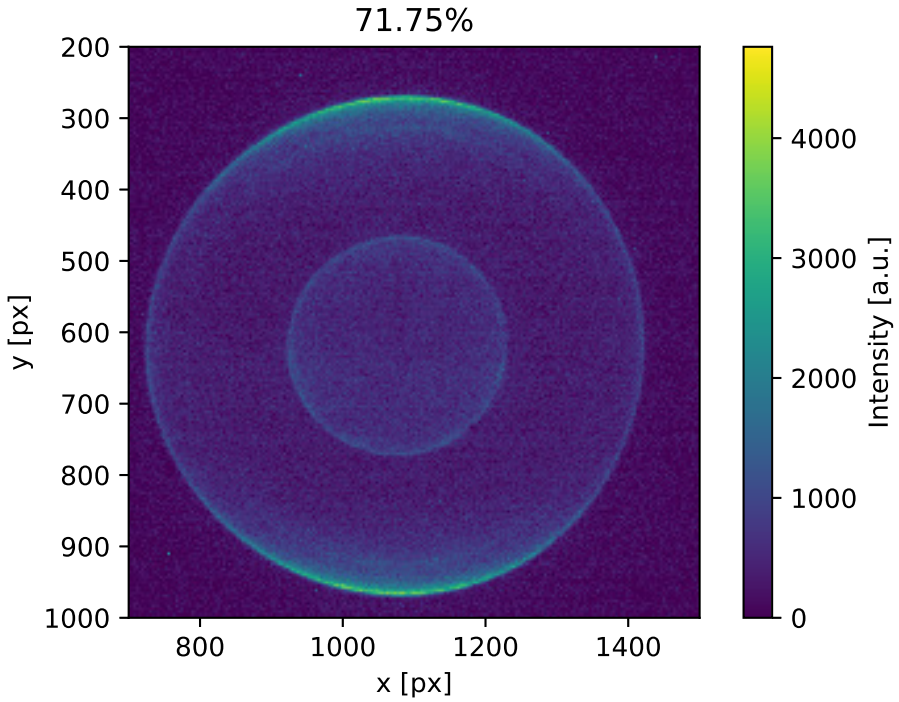

Fig. 5.9.: The summed picture at VMI mode at a voltage ratio of $U_E/U_R = 71.75\,\%$. It can be seen that the circle is slightly squashed in the y direction.

5.3.2. Photoelectron spectrum of Potassium

Next, only the photoelectron spectrum at the optimal ratio is looked at which can be seen in Fig. 5.10. A Gaussian is applied to the highest peak which yield an expectation value of

$$\mu_1 = 346.59(8)\,\text{px}$$

This peak can be identified as the kinetic energy which results out of the **REMPI** process. From

$$E_{\text{laser}} = E_{\text{kin}} + E_{\text{ion}} - E_{\text{level}} \tag{5.1}$$

with E_{laser} the energy of the laser, E_{kin} the kinetic energy of the electron, $E_{\text{ion}} = 4.340\,663\,54\,\text{eV}$ (see Fig. 1.2) and E_{level} as the energy level from which the electron got ionized follows

$$\mu_1 \equiv E_{\text{kin},1} = \frac{hc}{\lambda_{\text{laser}}} - \frac{hc}{\lambda_{5p_{3/2}\to\text{ion}}} = 1.755(3)\,\text{eV}$$

with $\lambda_{5p_{3/2}\to\text{ion}} = 946\,\text{nm}$ (from Fig. 1.6)

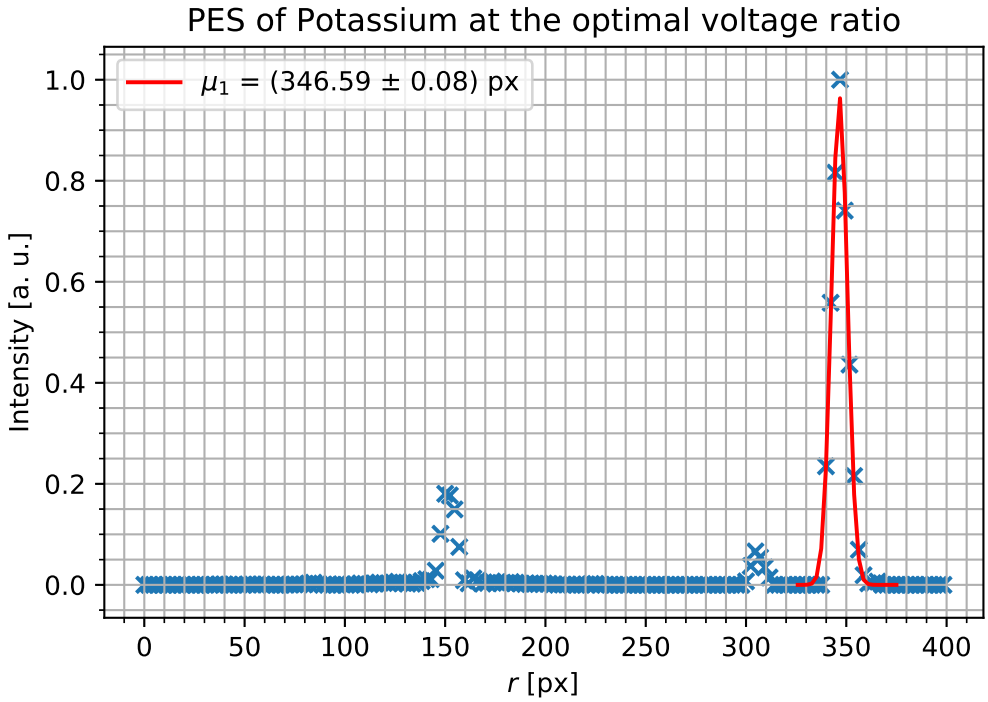

Fig. 5.10.: PES of Potassium at the optimal ratio. μ_1 is the expectation values of the fitted Gaussians which can be identified with the **REMPI** process.

Next, the pixels have to be transformed to kinetic energies so that the other peaks can be identified. The relation between energies and pixels is quadratic [3]

$$E_{\text{kin}}(r) = E_{\text{kin},1}\frac{r^2}{\mu_1^2}$$

In Fig. 5.11 the transformed plot can be seen. On each peak a Gaussian is applied to get the kinetic energies $E_{\text{kin},i}$ and their FWHM_i. The results are

$$\begin{aligned} E_{\text{kin},1} &= 1.7556(9)\,\text{eV} \\ \text{FWHM}_1 &= 0.095(2)\,\text{eV} \\ E_{\text{kin},2} &= 1.3659(14)\,\text{eV} \\ \text{FWHM}_2 &= 0.065(3)\,\text{eV} \\ E_{\text{kin},3} &= 0.3372(7)\,\text{eV} \\ \text{FWHM}_3 &= 0.038(2)\,\text{eV} \end{aligned}$$

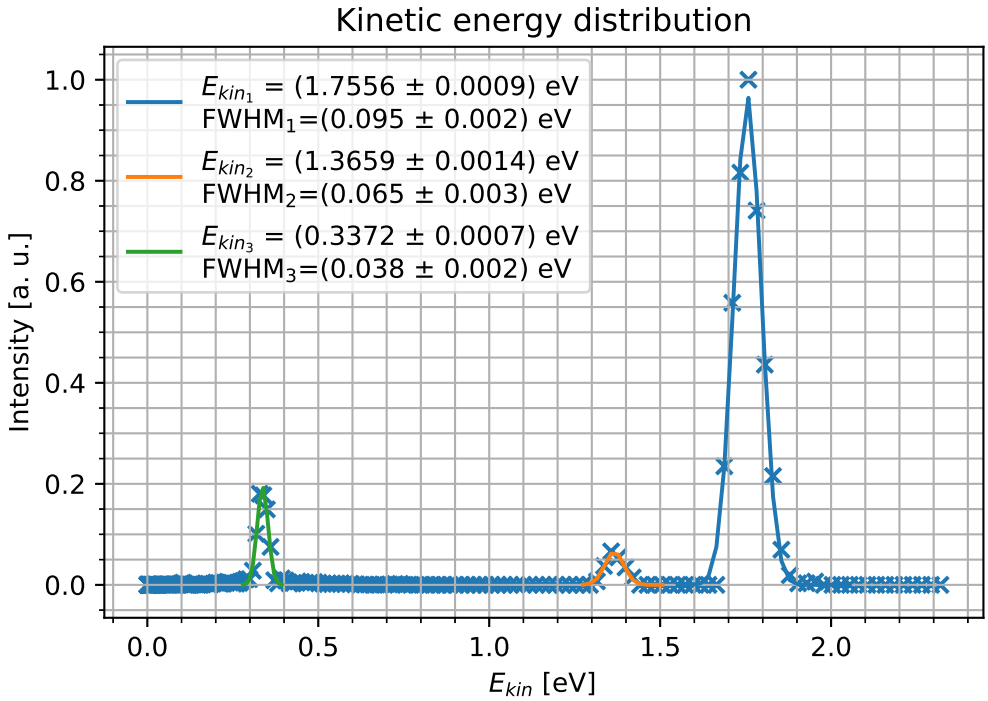

Fig. 5.11.: Kinetic energy distribution at the optimal voltage ratio. Gaussians are applied to get the kinetic energies and FWHMs corresponding to the peaks.

With (5.1) the energy levels can be computed to

$$E_2 = 2.64(3)\,\text{eV} \equiv E_{3d}$$
$$E_3 = 1.61(2)\,\text{eV} \equiv E_{4p}$$

where the uncertainty of the the energy is the standard deviation of the fitted peak, since the uncertainty of the laser energy and the Ionization energy are negligible. The identification follows from a comparison with known energy levels [4]

$$E_{3d} = 2.670\,\text{eV}$$
$$E_{4p} = 1.617\,\text{eV}$$

Next the resolution of the spectrum is determined. This is done by dividing the FWHMs by their corresponding kinetic energies

$$\delta E_1 = 5.41(12)\,\%$$
$$\delta E_2 = 4.8(2)\,\%$$
$$\delta E_3 = 11.2(5)\,\%$$

If one compares the measured energies with the theoretical values one can see that the measurements are in agreement. It was also shown that the resolution of the spectrometer is energy dependent which was expected.

5.3.3. Anistropy parameters

Finally the anisotropy parameters are estimated. For this, the output of pBasexL is transformed from pixels to energy as done above and the parameters are weighted with the normalised intensity of the PES of the according voltage ratio $U_E/U_R = 71.75\,\%$. For each transition the anistropy parameters are estimated by averaging all values that lie in the FWHM of the found peaks in Fig. 5.11 which are indicated as red vertical lines in Fig. 5.12.

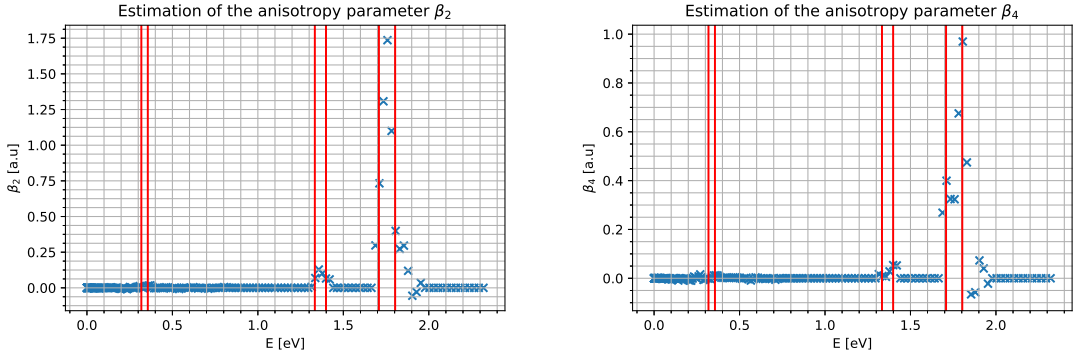

Fig. 5.12.: Estimation of the anisotropy parameter β_2 (left picture) and β_4 (right picture). The red lines indicate the FWHM of the peaks found in Fig. 5.11 and all entries that lie between two lines are averaged to get the parameter.

The results for the β_2 and β_4 can be found in Tab. 5.2 along with benchmark values taken from [6]. For the $5p_{3/2}$ state the anisotropy parameters have the expected magnitude. For the states $3d$ and $4p$ it can only be said that the anisotropy parameter β_4 is in the right order of magnitude while the measured β_2 seem to bee much too low. However, since we do not have useful uncertainties it might be that the measurement agrees with the theoretical values although this seems highly unlikely. A statistical error source could be again the fact that the center of the circle to get the inverted picture is only estimated by eye. However, this uncertainty cannot be quantified with the present data.

Tab. 5.2.: Anisotropy parameters for the different found transitions of Potassium

#	β_2	$\beta_{2,\text{theo}}$	β_4	$\beta_{4,\text{theo}}$
1	1.22	1.07(4)	0.43	0.52(8)
2	0.10	0.86(9)	0.015	0
3	0.005	0.17(3)	0.003	0

With these parameters the distribution for the absorption of polarized photons $J_{nl}(\theta)$ can be calculated via (1.10) and plotted which can be seen in Fig. 5.13 on the left. On the right the inverted picture of the recorded picture is shown and one can easily see that the intensity follows roughly the polar distribution from the right.

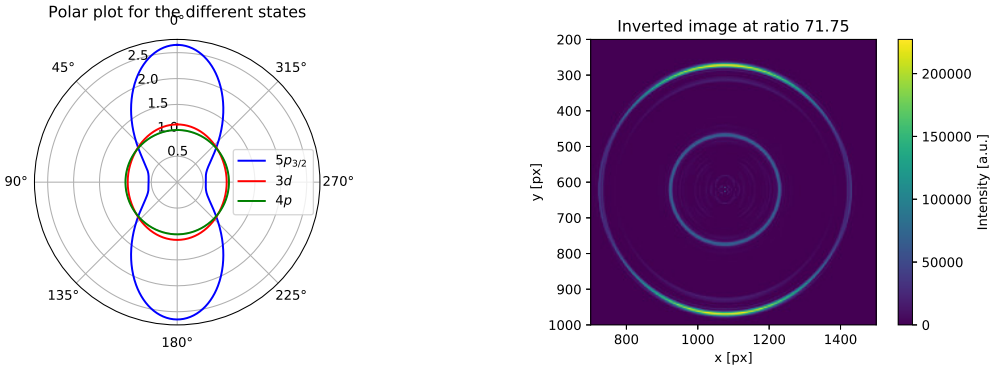

Fig. 5.13.: On the left: Distribution for the absorption polarized photons $J_{nl}(\theta)$ for all found transitions at the ratio 71.75%. On the right: Inverted picture at the same ratio.

6. Summary

6.1. Atom beam detector

By measuring the atomic flux with the LT-detector we discovered an exponential dependence on the oven temperature. The measurements have been executed at an atomic flux of roughly $5.5 \cdot 10^8\,\mathrm{atoms/s\,mm^2}$. We were not able to estimate the systematic uncertainties on the temperature and on the current. Our estimated statistical uncertainties were probably too low and it would have been more reasonable to use relative uncertainties.

6.2. Image ratio of the setup

In SMI mode we recorded different images by varying the lens distance to the atomic beam, thereby shifting the focal area of the laser. With this we were able to determine the image ratio to $\bar{B} = 89.8(7)\,\mathrm{px/mm}$.

6.3. Optimal voltage ratios

In the simulations we estimated the optimal voltages for SMI (VMI) by minimizing the distance on the detector between particles that had the same initial position (velocity) but different initial velocities (positions).
For SMI mode we applied Gaussians to the intensity distribution transversal to the propagation of the laser beam and plotted the resulting standard deviation over the voltage ratio $87\,\% \leq U_E/U_R \leq 92\,\%$ to find the minimum. Since there was no easy pattern recognizable the optimal voltage ratio was only estimated by eye.
In VMI mode the procedure was quite analogous. We used the photo-electron spectra given by the pBasexL program on which we applied Gaussians to the highest intensity peaks for voltage ratios between $70\,\% \leq U_E/U_R \leq 74\,\%$. Again the optimal ratio was only estimated by eye.
All obtained optimal ratios can be seen in Tab. 6.1.

Tab. 6.1.: Obtained optimal voltage ratios

	simulation	experiment
SMI	91.6030(14) %	89.6(4) %
VMI	72.688(5) %	71.8(4) %

6.4. Dimensions of the laser focal area

The beam waist and the Rayleigh length have been measured with two different methods. The results can be seen in Tab. 6.2. The values differ a lot from each other but the horizontal fit yields results of the same magnitude as the simulations, while the vertical fit results are not reasonable.

Tab. 6.2.: Obtained dimensions of the laser focal area

	Calculation	Vertical fit	Horizontal fit
w_0 [µm]	19.31(2)	63.3(13)	12.43(7)
z_R [mm]	2.896(3)	31.1(12)	1.201(13)
w_l [mm]	1	0.305(6)	1.553(9)

6.5. Photoelectron spectrum of Potassium

In VMI mode we measured different energy levels in the PES. In addition to the $5p_{3/2}$ level we could resolve the $3d$ and $4p$ levels but due to the resolution of the spectrum we were not able to determine the hyper fine structure. However, the found energy levels are in good agreement to the literature values. The resolution of the spectrum was also determined and all results can be seen in Tab. 6.3. The $5p_{3/2}$ energy was not "measured" since it provided the energy calibration of the setup.

Tab. 6.3.: Energy levels of Potassium

	measured	resolution	literature value
$5p_{3/2}$	-	5.41(12) %	3.065 eV
$3d$	2.64(3) eV	4.8(2) %	2.670 eV
$4p$	1.61(2) eV	11.2(5) %	1.617 eV

6.6. Anisotropy parameters

Last the anisotropy parameters have been estimated by the angular output of pBasexL. The results can be seen in Tab. 6.4. For the state $5p_{3/2}$ the obtained parameters seem to be reasonable while it did not work well for the other parameters.

Tab. 6.4.: Anisotropy parameters for the different found transitions of Potassium

#	β_2	$\beta_{2,\text{theo}}$	β_4	$\beta_{4,\text{theo}}$
1	1.22	1.07(4)	0.43	0.52(8)
2	0.10	0.86(9)	0.015	0
3	0.005	0.17(3)	0.003	0

Bibliography

[1] D. A. Dahl, J. E. Delmore, and A. D. Appelhans. "SIMION PC/PS2 electrostatic lens design program". In: *Review of Scientific Instruments* 61.1 (1990), pp. 607–609. DOI: 10.1063/1.1141932. eprint: https://doi.org/10.1063/1.1141932. URL: https://doi.org/10.1063/1.1141932.

[2] Bernhard Dick. "Inverting ion images without Abel inversion: maximum entropy reconstruction of velocity maps". In: *Phys. Chem. Chem. Phys.* 16 (2 2014), pp. 570–580. DOI: 10.1039/C3CP53673D. URL: http://dx.doi.org/10.1039/C3CP53673D.

[3] Lutz Fechner. "Aufbau eines Velocity-Map-Imaging-Spektrometers und winkelaufgelöste Spektroskopie an Rubidium-dotierten Helium-Nanotröpfchen". Albert-Ludwigs-Universität Freiburg, 2011.

[4] J. E. Sansonetti. "Wavelengths, Transition Probabilities, and Energy Levels for the Spectra of Potassium (KI through KXIX)". In: *Journal of Physical and Chemical Reference Data* 37.1 (2008), pp. 7–96. DOI: 10.1063/1.2789451. eprint: https://doi.org/10.1063/1.2789451. URL: https://doi.org/10.1063/1.2789451.

[5] A. Wituschek. *Versuchsanleitung Velocity Map Imaging*. 2016.

[6] A. Wituschek et al. "A simple photoionization scheme for characterizing electron and ion spectrometers". In: *Review of Scientific Instruments* 87.8 (2016), p. 083105. DOI: 10.1063/1.4960401. eprint: https://doi.org/10.1063/1.4960401. URL: https://doi.org/10.1063/1.4960401.

A. Lab notes

VMI

17.06.20

SimIon

~~Loaded PA instance geometry.~~

Loaded geometry: geometry.iob

To do: Find optimal ratio U_E/U_R (Repeller/Extractor) for VMI-mode

Fixed parameters ①

particles
$m_e = m_e$
$q = -e$
$x = y = z$
$y_1, y_2 = -0.5, 0.5$ mm
dir: $\vec{v} = (1, 0, 0)$
KE = 0.1eV
TOF = 0
CWF = 1
Colors: green, blue
$U_R = -3$kV
$\Delta x_{ini} = 1$mm

Tab 1.

U_E/kV	y_1/mm	y_2/mm	z_1/mm	z_2/mm
-1.5	-1.3291	1.3291	0	0
-1.8	-0.798435	0.798435	"	"
-2.1	-0.183625	0.183625	"	"
-2.4	0.537662	-0.537662	"	"
-2.7	1.3708	-1.3708	"	"
-2.2	0.0437899	-0.0437899	"	"
-2.250	0.162231	-0.162231	"	"
-2.15	-0.071457	0.071457	"	"
-2.181	0.0065687	-0.0065687	"	"

⇒ Best ratio U_E/U_R is around 72.8%.

Next: check, if the ideal ratio holds also for other U_R.

Tab 2.

U_R/kV	U_E/kV	y_1/mm
-3.5	-2.548	0.00656618
-4	-2.912	0.00652319
-4.5	-3.276	0.00645144
-5	-3.640	0.00635841
-2.5	-1.82	0.00651108
-2	-1.456	0.00063571

continuation of Tab 1 to get more points between $0.7 < U_E/U_R < 0.75$ (18.06.20)

U_E/kV	y_1/mm
-2.17	-0.0257343
-2.19	0.0204885
-2.21	0.067219
-2.22	0.0907769
-2.13	-0.116691
-2.12	-0.139119
-2.11	-0.161432
-2.14	-0.0941133

To do Simulate a bunch of electrons

Difference ~~of~~ to parameters in ⑧:

$y = 0$ ∀.

$n = 500$

direction: pupil

Pupil: sphere distr. Center: $x=0, y=0, z=0$

radius = 0.1

U_E = 4, 2, 1

Color = red, green, blue

~~U_R~~ $U_R = 3\,kV$

$U_E = -2.181\,kV$

To do Find the optimal ratio for SMI

fixed parameters:

$m = 39.0938\,u$

$q = +e$

$x = y = z = 0$

$\vec{v}_1 = (0,1,0)$; $\vec{v}_2 = (0,-1,0)$

$U_E = 0.1\,eV$

TOB = 0

CWF = 1

Color = blue, green

$U_R = 3\,kV$

Due to symmetry, only y_1 will be noted, as the distance will be twice of the absolute value of y_1.

Tab 3

U_E/kV	y_1/mm
1.5	5.35695
1.8	4.84034
2.1	4.0827
2.4	2.8679
2.7	0.578745
3	-5.89714
2.8	-0.740245
~~2.75~~	-0.0241515
2.74	0.104474
2.745	0.040687
2.747	0.0148682
2.748	0.00189268
2.74815	$-5.74304 \cdot 10^{-5}$

~~To do Simulate~~

~~2~~.741	0.0918025
2.742	0.0790885
2.743	0.0663511
2.744	0.0535908
2.746	0.0279295
2.749	-0.0111269
2.71	0.465824
2.72	0.341327
2.73	0.228588
2.76	-0.157348
2.77	-0.295256
2.78	-0.48146
2.79	-0.586375

⇒ ideal ratio is 91%

Todo Simulate a particle cloud that represents the ionisation value

$$w_0 = \frac{\lambda \cdot f}{\pi \cdot w_L} \quad ; \lambda = 405\,nm, f = 150\,mm, w_L = 1\,mm$$

$$= \frac{405 \cdot 150 \cdot 10^{-12}}{\pi \cdot 10^{-3}}\,m$$

$$= \frac{60750}{\pi}\,nm$$

$$= 19.34\,\mu m$$

$$z_R = \frac{\pi w_0^2}{\lambda} = \pi \frac{(19.34)^2}{405}\,mm$$

$$= 2.901\,mm$$

Measurements

- The optical components were already placed properly, thus we ~~directly fed the laser directly~~ first checked whether the beam pathway is correct or whether it needs some corrections. This ~~was~~ the case
The beam pathway ~~was~~ fine, we only changed the $\lambda/2$-plate and mirrors a little.

To do Tune the laser to the correct frequency
In order to get the right frequency, we are changing the voltage of the piezo-crystal and the current in the diode. ~~Heater~~
After going through nearly all possible combinations, the Li-cell was still not glowing.
Thus the tutor changed the grid manually.
Afterwards the camera to observe the Li-cell crashed.
Next we are checking the wavelength with a spectrometer as we cannot observe the Li-cell any more.

19.06.20

Laser properties (spectrometer):
404.2nm ≙ max
1nm ≙ width ≙ FWHM

alle adjustment: 404.4nm ≙ max
1nm ≙ width ≙ FWHM

To do Obtain first image with the spectrometer

$U_{MCP} = 1700\,V$ $\quad \Delta U_{MCP} = 0.5\,V$
$U_R = 5000\,V$ $\quad \Delta U_R = 0.5\,V$
$U_{Ph} = 3500\,V$ $\quad \Delta U_{Ph} \approx 20\,V$
$T_{Kryo} = 148.8\,°C$ (temperature is continuously decreasing)
$U_E/U_R = 89.6\,\%$ $\quad \Delta \frac{U_E}{U_R} \approx 0.2\,\%$

Laser: ~~$A = 51.0\,mA$~~
~~$A = 50.996$~~
$A = 50.78463\,mA$
$U = 38.38\,V$

To do ~~Final adjustment~~ Determine the image ratio

$T_{start} = 146.4\,°C$

Tab 4

#	d/mm
0	5.00
1	5.50
2	6.00
3	6.50
4	7.00
5	5.14
6	4.50

~~n0 = 5,00~~
~~n1 = 5,50~~
~~n2 = 6,00~~
~~n3 = 6,50~~
~~n4 = 7,00~~
~~n5 = 7,50~~
~~n6 = 4,0~~

Last laser setting: $T_{end} = 146.6\,°C$

I = 51.03620 mA

U = 37.27 V

To do Determine optimal ratio U_E/U_R for SMI

T_{start} 142.9 °C

laser start setting

I = 51.87317 mA; U = 33.02 V

Tab 5

#	ratio / %	
0	89.6	
1	92.0	$I_{start,1} = 51.78317\,mA$, $U_{start} = 33.02\,V$
2	~~88~~ 87	$I_{start,2} = 51.83\,mA$, $U_{start} = 33.02\,V$
3	88	$I_{start,3} = 51.54317\,mA$, $U_{start,3} = "$
4	89	$I_{start,4} = 51.49317\,mA$, $U_{start,4} = "$
5	90.0	$I_{start,5} = 51.45317\,mA$, $U_{start,5} = "$
6	91.0	$I_{start,6} = 51.36317\,mA$, $U_{start,6} = "$
7	89.3	$I_{start,7} = 51.35317\,mA$, $U_{start,7} = "$

$T_3 = 141.8\,C$

To do: Measure the atomic flux vs. the oven temperature

$U_{Exc} = 7.9\,V$; $U_{Rep} = 14.9\,V$ $\Delta U = 0.1\,V$

Nanoamperemeter is set to 10nA-display

$\Delta I = 0.01\,nA$

$\Delta T = 0.2\,K$

Tab 6

T/°C	I/nA	T/°C	I/nA
159.2	2.570	137	0.440
159.0	2.130	136	0.400
158.0	1.760	135	0.38
157.0	1.630	134	0.37
156.0	1.420	133	0.35
155.0	1.360	132	0.32
154.0	1.260	131	0.30
153.0	1.180	130	0.28
152.0	1.110	129	0.26
151.0	1.060	128	0.24
150.0	1.040	127	0.22
149.0	0.930	126	0.20
148.0	0.900	125	0.19
147.0	0.780	124	0.18
146.0	0.770	123	0.16
145.0	0.720	122	0.15
144.0	0.680	121	0.13
143.0	0.640	120	0.12
142.0	0.600	119	0.11
141.0	0.580	118	0.10
140.0	0.540	117	0.09
139.0	0.520	116	0.09
138.0	0.47	115	0.08

#	ratio
0	71.5
1	70.0
2	73.0
3	74.0
4	73.5
5	~~72.5~~ 72.5
6	72.0
7	72.25
8	72.75
9	71.75
10	71.25

optimal voltage ratio for VMI

$T = 14.3\,^{\circ}C$

$T_{base} = 19.820\,^{\circ}C$

To reduce the background, another image ~~of~~ is taken. ~~For this, the laser is~~

For this picture, only the MCPs and the phosphor screen ~~one~~ are switched on to 1.74kV/3.5kV and the laser ~~is~~ is emitting.

B. Tables

Tab. B.1.: Results of the Gaussian fits

lens postion [mm]	cut position [px]	μ [px]	s_μ [px]
4.5	993.0	614.1	0.2
5.0	993.0	659.1	0.2
5.5	1031.0	705.4	0.3
6.0	1045.0	749.2	0.3
6.5	1027.0	793.8	0.3
7.0	1015.0	838.8	0.3

Tab. B.2.: Determination of the image ratio at SMI setting

transition	Δx [mm]	$s_{\Delta x}$ [mm]	Δd [px]	$s_{\Delta d}$ [px]	B [px / mm]	s_B [px / mm]
4.5mm→5.0mm	0.50	0.01	44.9	0.3	89.8	1.4
5.0mm→5.5mm	0.50	0.01	46.3	0.4	92.6	1.5
5.5mm→6.0mm	0.50	0.01	43.9	0.4	87.8	1.5
6.0mm→6.5mm	0.50	0.01	44.6	0.4	89.2	1.5
6.5mm→7.0mm	0.50	0.01	44.9	0.4	89.8	1.5

Tab. B.3.: Results of the Gaussian fits for optimal ratio

U_E/U_R [%]	cut position [px]	σ [px]	s_σ [px]
87.0	986	6.05	0.12
88.0	1013	4.51	0.07
89.0	1042	3.12	0.06
89.3	1025	2.97	0.05
89.6	918	2.84	0.05
90.0	1009	2.88	0.05
91.0	1012	4.47	0.07
92.0	1001	6.73	0.11

C. Figures

C.1. Summed pictures with subtracted background at VMI mode

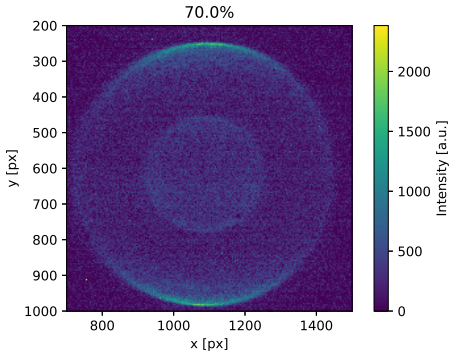

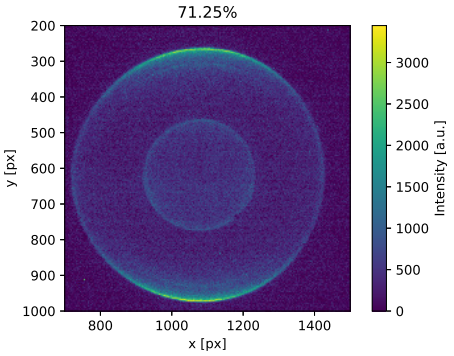

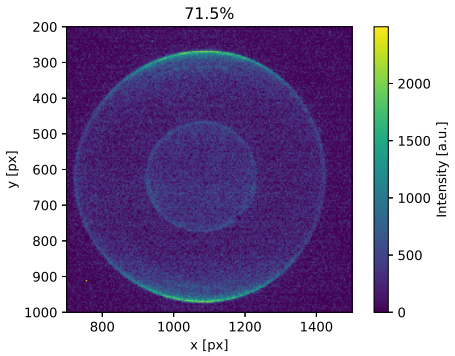

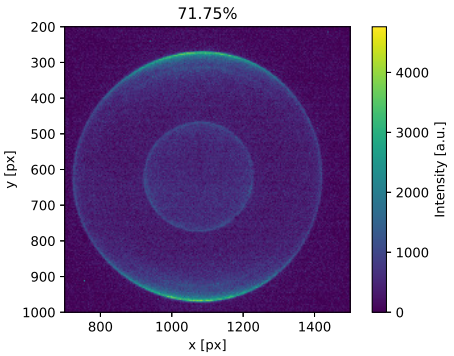

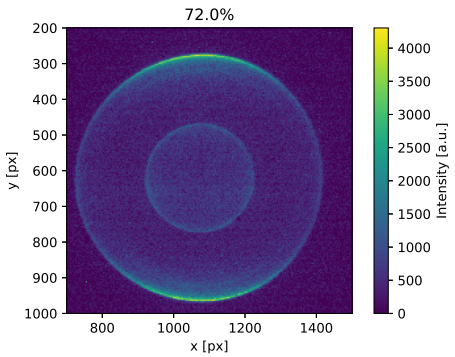

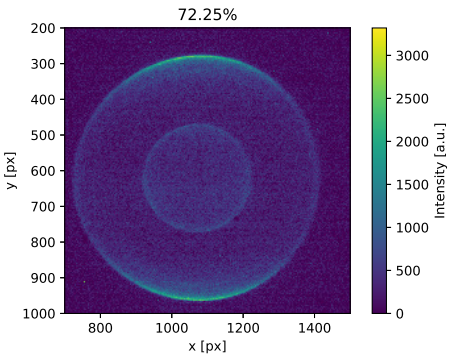

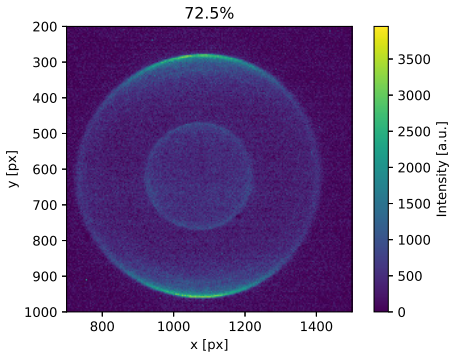

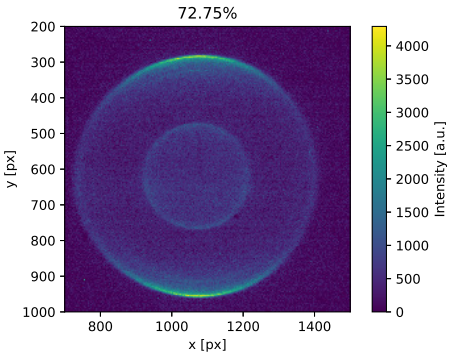

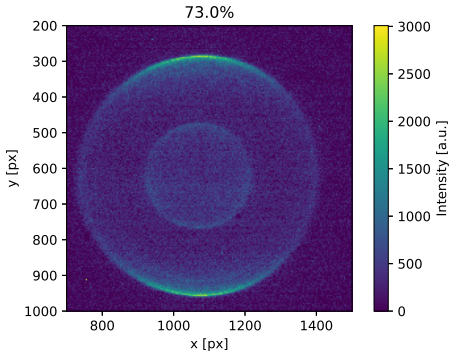

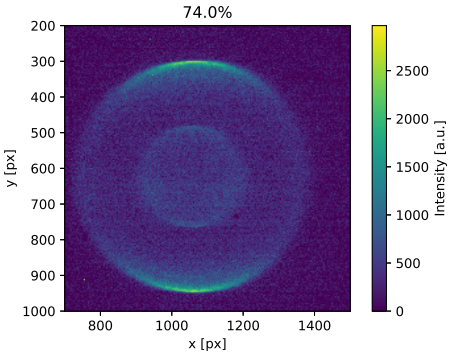

C.2. Figures for 5.2.1

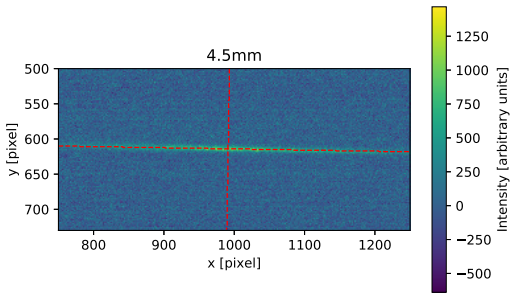

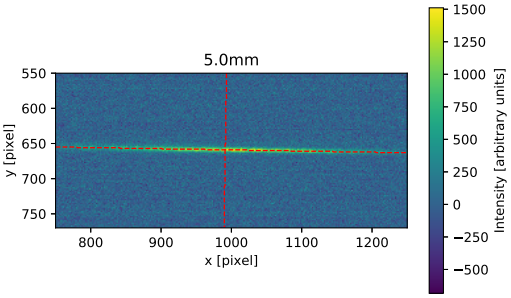

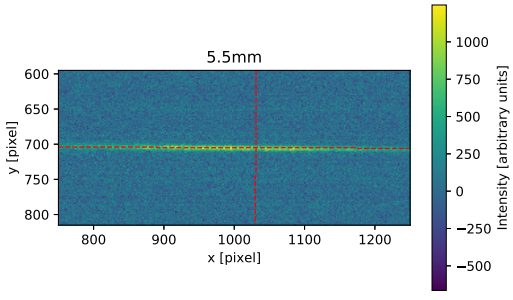

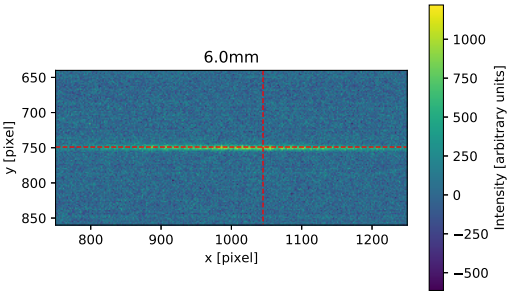

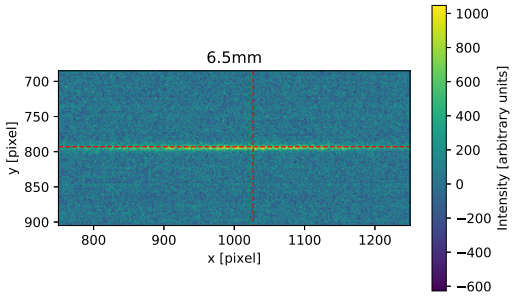

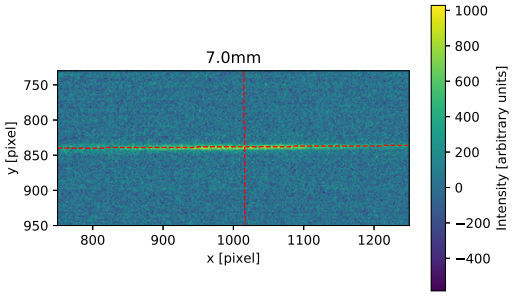

C.3. Figures for 5.2.2

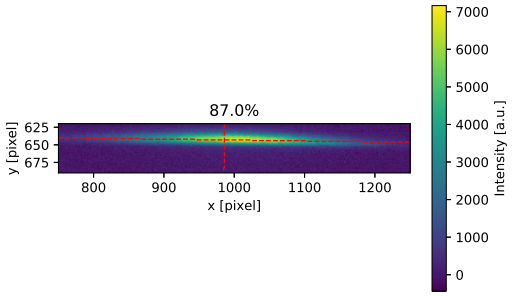

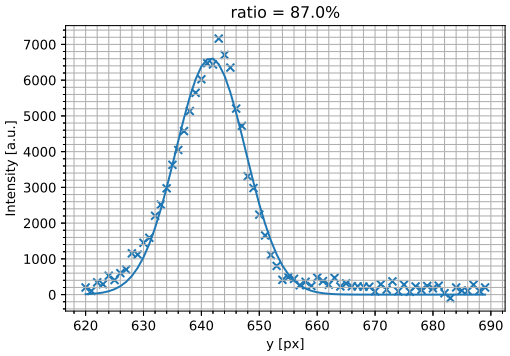

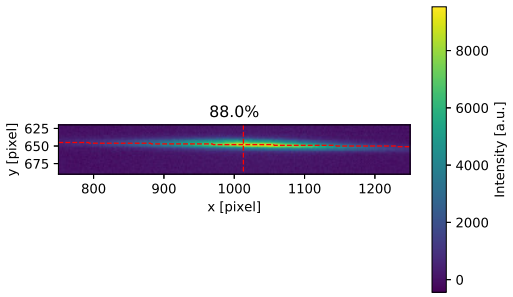

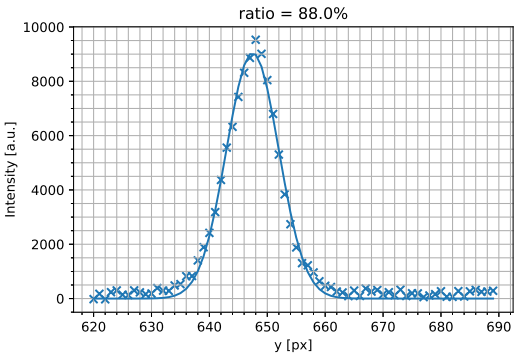

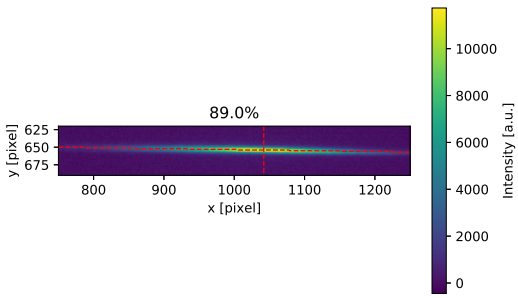

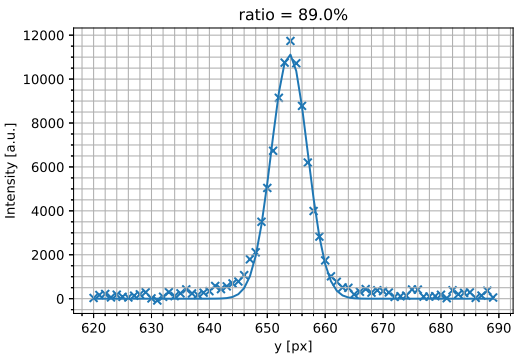

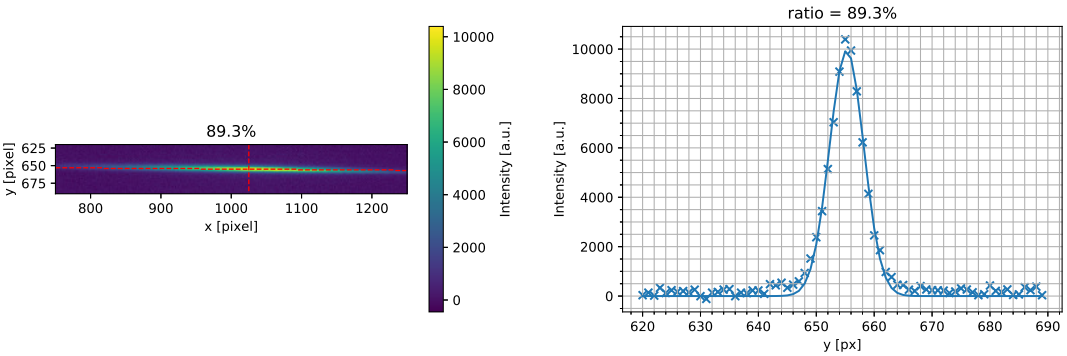
89.3%
y [pixel]
x [pixel]
Intensity [a.u.]
ratio = 89.3%
Intensity [a.u.]
y [px]

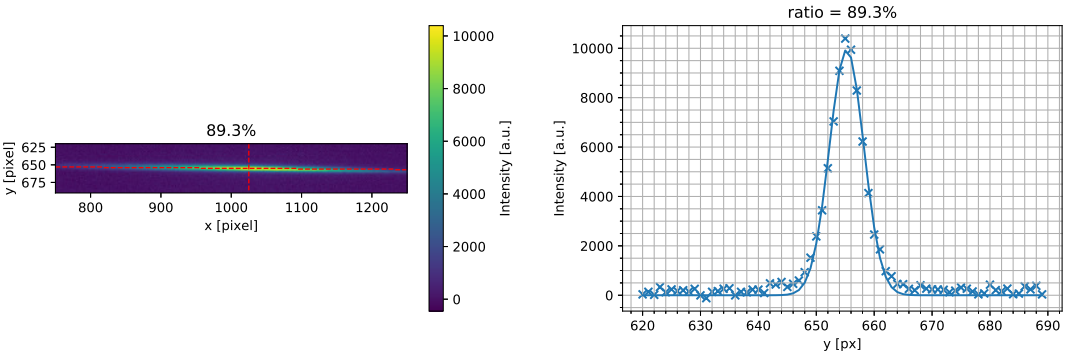
89.3%
y [pixel]
x [pixel]
Intensity [a.u.]
ratio = 89.3%
Intensity [a.u.]
y [px]

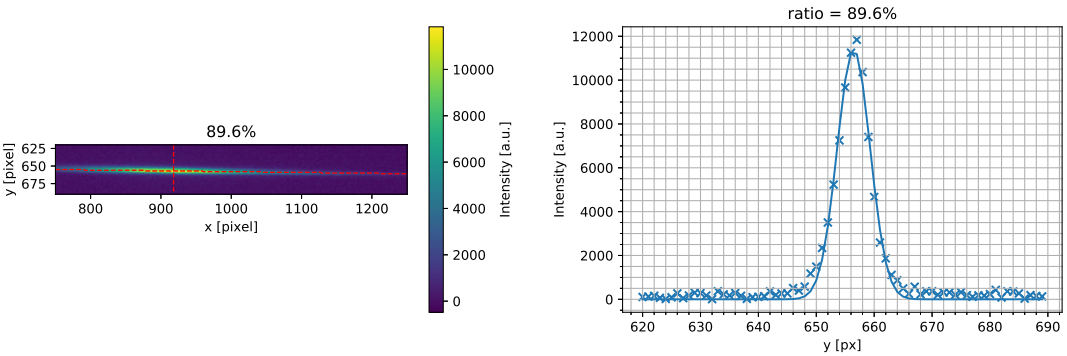
89.6%
y [pixel]
x [pixel]
Intensity [a.u.]
ratio = 89.6%
Intensity [a.u.]
y [px]

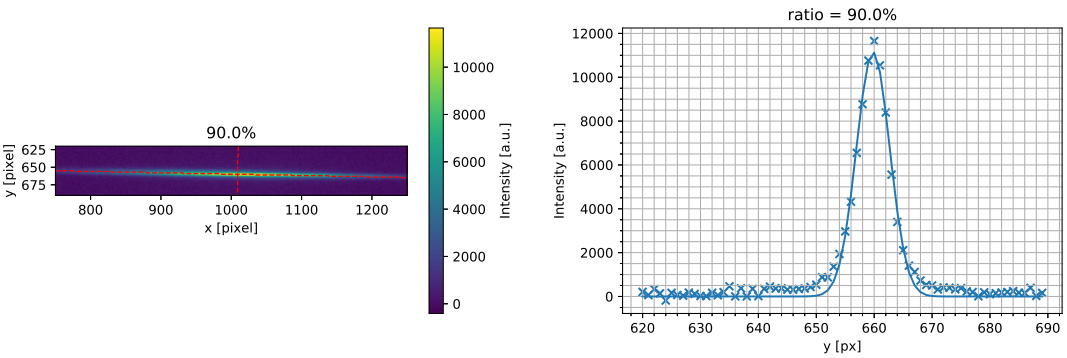
90.0%
y [pixel]
x [pixel]
Intensity [a.u.]
ratio = 90.0%
Intensity [a.u.]
y [px]

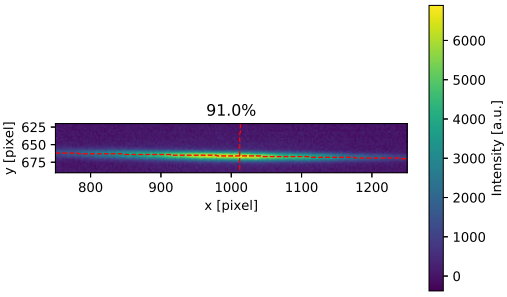

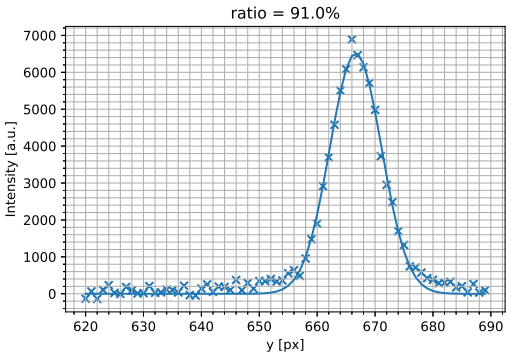

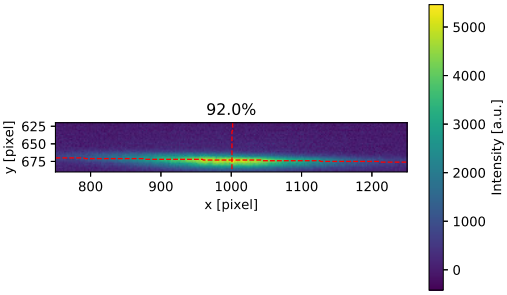

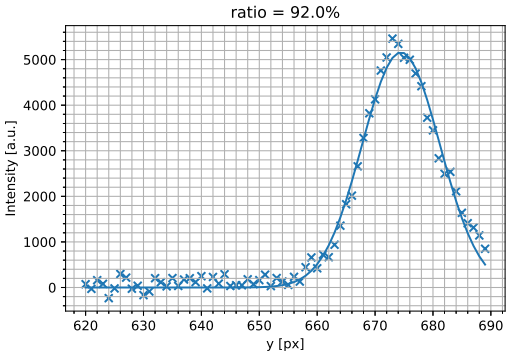

C.4. Figures for 5.3.1

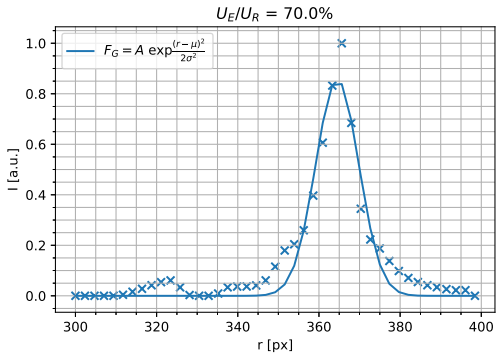

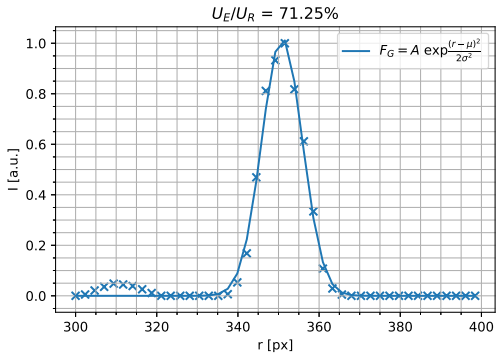

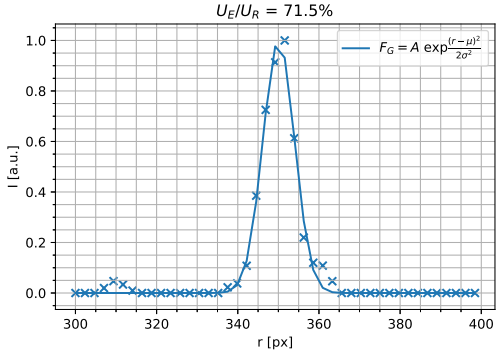

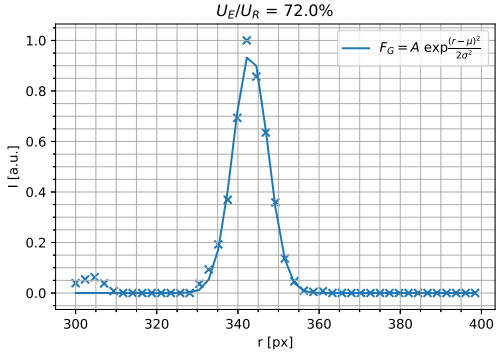

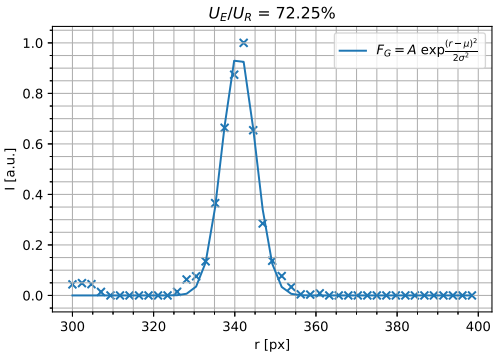
U_E/U_R = 72.25%
$F_G = A \exp\frac{(r-\mu)^2}{2\sigma^2}$
I [a.u.]
r [px]

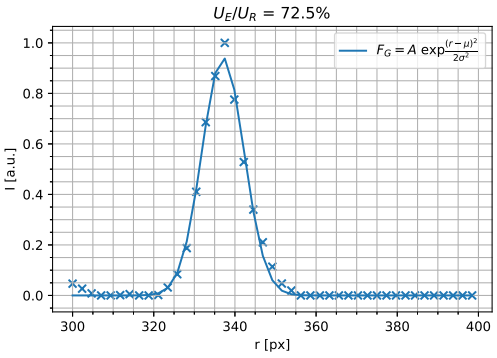
U_E/U_R = 72.5%
$F_G = A \exp\frac{(r-\mu)^2}{2\sigma^2}$
I [a.u.]
r [px]

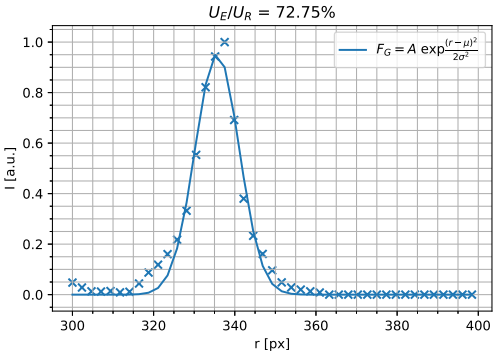
U_E/U_R = 72.75%
$F_G = A \exp\frac{(r-\mu)^2}{2\sigma^2}$
I [a.u.]
r [px]

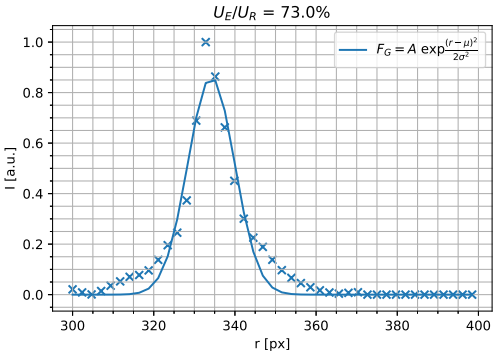
U_E/U_R = 73.0%
$F_G = A \exp\frac{(r-\mu)^2}{2\sigma^2}$
I [a.u.]
r [px]

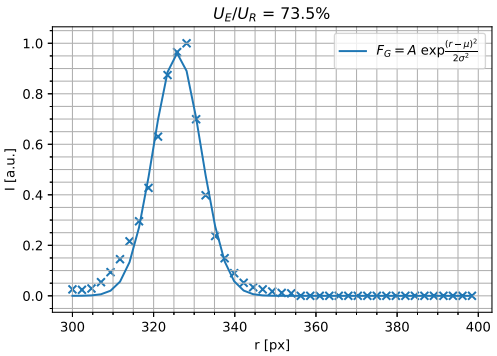
U_E/U_R = 73.5%
$F_G = A \exp\frac{(r-\mu)^2}{2\sigma^2}$
I [a.u.]
r [px]

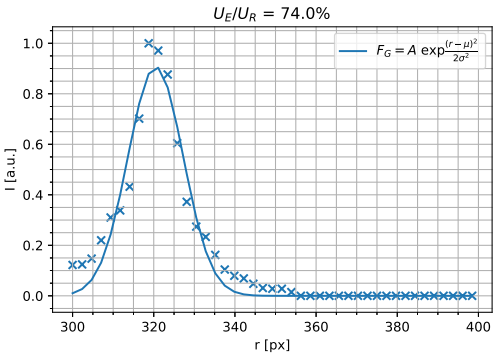
U_E/U_R = 74.0%
$F_G = A \exp\frac{(r-\mu)^2}{2\sigma^2}$
I [a.u.]
r [px]